Summer 2016

Proactive strategies in personal dose monitoring, prevention and mitigation

Manish Kumar Sharma

Department: Mining and Nuclear Engineering

PROACTIVE STRATEGIES IN PERSONAL DOSE MONITORING, PREVENTION AND MITIGATION

by

MANISH KUMAR SHARMA

A DISSERTATION

Presented to the Graduate Faculty of the

MISSOURI UNIVERSITY OF SCIENCE AND TECHNOLOGY

In Partial Fulfillment of the Requirements for the Degree

DOCTOR OF PHILOSOPHY

in

NUCLEAR ENGINEERING

2016

Approved by

Dr. Ayodeji B. Alajo, Advisor
Dr. Hyoung K. Lee
Dr. Xin Liu
Dr. Shoaib Usman
Dr. Mahelet Fikru

PUBLICATION DISSERTATION OPTION

This dissertation has been prepared in the form of four journal papers, formatted in the style used by Missouri University of Science and Technology.

Pages 5 to 28, "Three-dimensional Localization of Low Activity Gamma-Ray Sources in Real-Time Scenarios," have been published in *Nuclear Instruments and Methods in Physics Research Section A* (2016).

Pages 29 to 56, "MCNP Modeling of a Neutron Generator and its Shielding at Missouri University of Science and Technology," have been published in *Nuclear Instruments and Methods in Physics Research Section A* (2014).

Pages 57 to 82, "Adjoint Acceleration of Monte Carlo Simulations using SCALE: A Radiation Shielding Evaluation of the Neutron Generator Room at Missouri S&T," have been published in *Nuclear Instruments and Methods in Physics Research Section A* (2015).

Pages 83 to 99, "Integrated Doses Calculation in Evacuation Scenarios of The Neutron Generator Facility at Missouri S&T," have been published in *Nuclear Instruments and Methods in Physics Research Section A* (2016).

ABSTRACT

At certain threshold, nuclear radiation (like x-rays and gamma-rays) may adversely impact the health of living tissues. The exposure to these radiations in nuclear facilities is measured by devices called dosimeters. The devices are generally worn on the torso and are monitored by health physics division to report the radiation dose received by the personnel. However, this approach is not proactive—since the dosimeters reflect the dose that has already been absorbed in the body of the wearer.

This work presents a scheme to proactively avoid large dose acquisition at radiation-prone facilities. The work was divided into three major segments: (i) identify and characterize radioactive source(s), (ii) determine the impact of localized source(s), and (iii) estimate the integrated doses in traversing/evacuating the facility. The scope of this work does not extend to the development of "proactive" dosimeter. However, the approaches developed in these segments will be integrated into a dose monitoring system that would prevent or mitigate large dose acquisition. This work also has applications in nuclear facilities, hospitals, homeland security, and border protection.

ACKNOWLEDGMENTS

This is the time to acknowledge those persons who have been a crucial part of my success. I would start by thanking my advisor, Dr. Ayodeji Alajo. His "young" approach in dealing and solving the problems has always admired me. He did his best to nurture my thinking process. Not only he focused on my academic and research skills but he also silently shaped my professional and leadership skills. My passion to work with him never died just because of the confidence and trust he had in me and my abilities. I am also deeply grateful to Dr. Hyoung Lee and Dr. Xin Liu for their outstanding co-advising. The projects they have co-advised are the crux of this work.

It was in the year 2010 when I decided to obtain a doctoral degree. I was inspired by Dr. Prabhat Munshi's dedication to the field of Nuclear Engineering. Through his unbiased suggestions, he has played an integral role in building my academic career. I would now like to acknowledge those who always believed that I am a Rockstar—my family and friends. I am thankful to my parents for giving the birth to an awesome kid—me! This work is dedicated to all the rough times we have been through. Preparing for the IIT examination was the moment when my brother, sister, and sister-in-law motivated me to give my best shot. I would have got lost in the crowd, otherwise. My time at Rolla was made enjoyable by my best buddies: Shashank, Aditi, Vimal, and Ashish. This work is incomplete without mentioning them. The funding from U.S. Nuclear Regulatory Commission and Dissertation Completion Fellowship Program is greatly acknowledged as well. Lastly, this work is dedicated to my alma mater, IIT Kanpur, for training me to demonstrate perfection in every task I undertake. With this in my mind, I now declare to become the third doctor in my family.

TABLE OF CONTENTS

Page

LIST OF ILLUSTRATIONS

LIST OF TABLES

1. INTRODUCTION

The exposure to nuclear radiations (like x-rays and gamma-rays) in radiation-prone facilities is monitored with devices called dosimeters. Since the ionizing radiations lie in the high-energy region of the electromagnetic spectrum, the personnel may inadvertently be exposed to these radiations. Therefore, dosimeters play an integral role in radiation protection by ensuring that the dose levels are below the permissible limits. These devices are generally worn on the outside of the clothing and around the torso. This approach of dose monitoring, however, is not proactive since the dose information is available after the fact; the dosimeters reflect the dose that has already been acquired by the wearer. Moreover, it is always desired to keep the dose levels low in accordance with the ALARA* principle. Hence, any proactive planning and development of proactive strategies could help in dose minimization; in favor of the ALARA principle. This section presents the current strategy employed in personal dose monitoring and the proposed concepts and schemes to prevent and mitigate large dose acquisitions in radiation-prone facilities.

1.1. CURRENT STRATEGY EMPLOYED IN PERSONAL DOSE MONITORING

The current strategy employed in dose monitoring primarily consists of following four steps.

1. The personnel is provided a dosimeter by the facility staff. This device is worn on the torso.
2. The device is returned to the staff before personnel leaves the facility.
3. The device is sent to the health physics division.
4. The health physics division then reports the dose acquired by the personnel during the time of exposure.

*ALARA is the acronym for **A**s **L**ow **A**s **R**easonably **A**chievable radiological safety principle.

It could even take few months to get the dose acquisition report; hence, this approach is not proactive. Further, the personnel has already been exposed to the radiation and has no control over the acquired dose.

1.2. PROPOSED APPROACH FOR PERSONAL DOSE MONITORING

The focus of present work is to improve the current strategy of dose monitoring and reduction. The idea is to replace the dosimeter with more smart (electronic) device, which provides information of source terms (e.g., location, strength, and dose-map of radioactive sources) in the facility. This information will be available to each personnel in near real-time—to avoid radiation-prone areas. To achieve this goal, the work was divided into three segments (see Figure 1.1). The approaches developed in these segments will eventually be integrated into a monitoring system to prevent and mitigate large dose acquisitions.

Segment I. Identify, localize, and characterize the radioactive source(s) in the facility.

Segment II. Predict the impact of the localized source(s) (i.e., the dose-map).

Segment III. Calculate the integrated doses and determine the safest path—with least dose acquisition—for each personnel using the dose-map.

Once the final information is available (i.e., the decision made at point A of Figure 1.1), there exists no technological gap for its dissemination in near real-time. For example, the personnel can be alerted through a text message on their cell phones or through any radio frequency (RF) device.

Paper I of this dissertation presents an algorithm to achieve the first objective. The algorithm utilizes the responses (counts) at various known detector positions for three-dimensional localization of gamma-ray sources in real-time. The algorithm was verified using Monte Carlo N-Particle (MCNP) radiation transport code [1] and was validated through experiment. The simulation and experimental results were also compared with well-established least squares method [2]. Since the algorithm was validated with weak

laboratory source (^{137}Cs source of strength 5.1 μCi), it had considerably lower doses in its vicinity. A radiation-prone facility, however, should have a stronger source of ionizing radiations. Since the algorithm successfully localized the weak source, it is believed that it will detect and characterize the stronger radioactive sources in real-time.

For impact prediction in Segment II, a more realistic case of higher activity source—a neutron generator emitting stronger ionizing radiations—was considered. The accelerator-type neutron generator, at Missouri University of Science and Technology, utilizes D-D fusion reactions to produce neutrons of approximate energy 2.5 MeV. The generator, its shielding, and its room of operation were modeled using MCNP for impact (dose-rate) prediction (Paper II). Since the Monte Carlo simulation was computationally expensive, it was later accelerated using automated variance reduction sequence (MAVRIC) of the SCALE package [3]. This work (presented in Paper III of this dissertation) was cardinal for near real-time implementation of the final scheme.

The decision making approach primarily comprises of determination of safest route—with least dose acquisition—for each personnel of the facility. To achieve this objective, the neutron generator model was further extended to cover the entire floor of the building. The idea was to determine the dose rates in the hallways of the building, which would be used to test the decision making (dose reduction) approach (see Figure 1.2). This

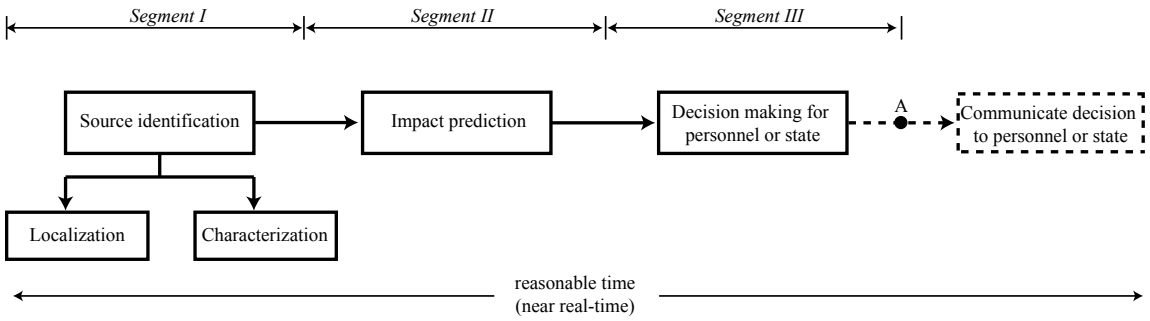

Figure 1.1 Segments of the proposed research.

approach, discussed in Paper IV, calculates the integrated dose acquired in traversing the facility to distinguish the safest path to exit the building.

As discussed previously, the approaches presented in Papers I-IV of this dissertation will be integrated to prevent and mitigate large dose acquisitions. Beyond dose minimization, this work has applications in nuclear facilities, hospitals, homeland security, and border protection.

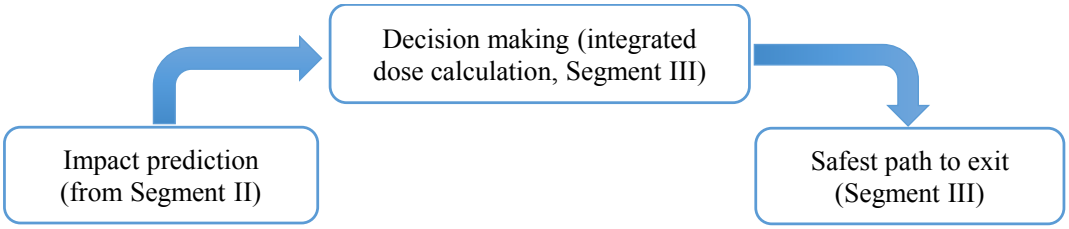

Figure 1.2 Decision making and determination of safest path (Segment III).

PAPER

I. THREE-DIMENSIONAL LOCALIZATION OF LOW ACTIVITY GAMMA-RAY SOURCES IN REAL-TIME SCENARIOS

Manish K. Sharma, Ayodeji B. Alajo, Hyoung K. Lee

Missouri University of Science & Technology,

Nuclear Engineering, Rolla, MO, USA

ABSTRACT[†]

Radioactive source localization plays an important role in tracking radiation threats in homeland security tasks. Its real-time application requires computationally efficient and reasonably accurate algorithms even with limited data to support detection with minimum uncertainty. This paper describes a statistic-based grid-refinement method for backtracing the position of a gamma-ray source in a three-dimensional domain in real-time. The developed algorithm used measurements from various known detector positions to localize the source. This algorithm is based on an inverse-square relationship between source intensity at a detector and the distance from the source to the detector. The domain discretization was developed and implemented in MATLAB. The algorithm was tested and verified from simulation results of an ideal case of a point source in non-attenuating medium. Subsequently, an experimental validation of the algorithm was performed to determine the suitability of deploying this scheme in real-time scenarios. Using the measurements from five known

[†]Published in Nuclear Instruments and Methods in Physics Research Section A (2016).

detector positions and for a measurement time of 3 minutes, the source position was estimated with an accuracy of approximately 53 cm. The accuracy improved and stabilized to approximately 25 cm for higher measurement times. It was concluded that the error in source localization was primarily due to detection uncertainties. In verification and experimental validation of the algorithm, the distance between ^{137}Cs source and any detector position was between 0.84 m and 1.77 m. The results were also compared with the least squares method. Since the discretization algorithm was validated with a weak source, it is expected that it can localize the source of higher activity in real-time. It is believed that for the same physical placement of source and detectors, a source of approximate activity 0.61-0.92 mCi can be localized in real-time with 1 second of measurement time and same accuracy. The accuracy and computational efficiency of the developed scheme make this algorithm a suitable candidate for its deployment in real-time localization of radioactive sources.

Keywords: Radiation source localization, Nuclear nonproliferation, Domain discretization, Border protection, Radiation detection, Scintillation detector

1. INTRODUCTION

The detection and identification of radioactive material is an important aspect of both nuclear safeguard and material protection. One of the key aspects in nuclear material surveillance is the identification and localization of the radioactive sources in real-time. Computational schemes are continually developed to facilitate such surveillance. The algorithm used to track the radiation source should be computationally efficient to facilitate early detection in near real-time, without sacrificing accuracy.

In previous studies, the geometric difference triangulation method was used to locate radiation sources [1]. The measurements collected from three sensors were used to estimate the source location and its strength. Howse et al. [2] discussed recursive and the moving horizon non-linear least squares estimation algorithms for the real-time estimation of a moving source. This work incorporated the use of four gamma-ray detectors located at four different positions of the monitoring area. The algorithm developed was used to track the location of the moving source within that region. The results were presented for a ^{137}Cs source moving along a predetermined path. For efficient collection of data, the approximate measurement time was 3 minutes at each point the source was stopped.

RadTrack, developed at Argonne National Laboratory, uses a combination of a set of radiation detectors and a video camera to track a radioactive source [3]. It utilizes a map of probability density function to localize the radiation source. The results were presented for both a 1 mCi ^{60}Co source and a relatively weak (100 μCi) ^{137}Cs source. For the 100 μCi source, the method of temporal linking reduced the mean error in estimation to approximately 0.9 m.

Chin et al. [4] have addressed the problem in localization of low-level radioactive sources under realistic noise and measurement errors. For the performance evaluation of their iterative pruning (ITP) fusion algorithm, the results were reported for a ^{137}Cs source of extremely low activity of 0.911 μCi. The simulation results compare the localization

error for different source strengths and sensor densities. For a 400 μCi source and sensor density of approximately 1 per 1100 m^2 area, the algorithm localized the source within 32.5 m. Circles of Apollonius could also be used in source localization [5]. This study discussed a key problem—i.e., ambiguity (non-uniqueness)—in the position estimates and how an additional detector distinguishes the actual source position. The analysis considered an ideal scenario with no statistical fluctuations.

A particle filter algorithm was proposed by Rao et al. [6] to detect radioactive sources. The outputs of this algorithm demonstrates the benefits of networked configuration over the non-networked and pair configurations of the counters. In this work, results were presented for a notional border monitoring scenario with twelve 2 in. $\times$ 2 in. NaI detectors. Another class of localization algorithms that has been explored extensively in the literature utilizes Difference of Time-of-Arrival (DTOA) method [7–9]. Linear algebraic approach for localization using DTOA method is addressed in [9, 10]. Some other works that are relevant to the work presented in this paper are discussed in [11–13].

This paper introduces a new, simpler, and faster approach to predict the source position in a three-dimensional domain. The algorithm is also proposed for use in real-time backtracing applications. The suitability of this algorithm for real-time applications required it to be fast and accurate even with limited data.

2. SOURCE POSITION PREDICTION METHODOLOGY

Radiation intensity $I(x_i, y_i, z_i)$ at a particular position (x_i, y_i, z_i), due to a localized radiation source, in a non-attenuating medium, is inversely proportional to the square of its distance from the source:

$$I(x_i, y_i, z_i) \propto \frac{S(x, y, z)}{r_i^2} \tag{1}$$

where r_i is the distance from the i^{th} position to a radiation source of strength S at position (x, y, z).

The generalization of Eq. (1) for various detector positions is

$$I_1 r_1^2 = I_2 r_2^2 = \ldots = I_i r_i^2 = S * K \tag{2}$$

where K is a constant of proportionality, I_i is the intensity at the i^{th} position and r_i is the distance from this position to the source (see Figure 2.1).

Gunatilaka et al. [12] explained a general case for estimation of a source position in a two-dimensional domain. In a real-world situation where the source may be placed above the ground, i.e. where the discrimination in z-direction becomes important, backtracing in three-dimensional space will give a better insight of the source positioning. The localization of radioactive source becomes more rigorous in this scenario. The equation of any sphere centered at a detector position (x_1, y_1, z_1) and passing through the source position (x, y, z) is given by

$$(x - x_1)^2 + (y - y_1)^2 + (z - z_1)^2 = r_1^2 \tag{3}$$

where r_1 is the radius of the sphere. In general, the equation of any sphere with radius r_i centered at the detector position (x_i, y_i, z_i) and passing through the source position (x, y, z) is

$$(x-x_i)^2 + (y-y_i)^2 + (z-z_i)^2 = r_i^2, \text{ for all } i = 1,2,3,4\ldots \tag{4}$$

If it is assumed that there is no attenuating medium in the line of sight of the detector, and the intensity at a position perfectly follows the inverse-square relationship, then

$$r_i^2 = \left(\frac{I_1}{I_i}\right) r_1^2 \equiv k_{1i} r_1^2, \text{ where } k_{1i} = \left(\frac{I_1}{I_i}\right) \tag{5}$$

Combining Eq. (4) and Eq. (5), creates

$$(x-x_i)^2 + (y-y_i)^2 + (z-z_i)^2 = k_{1i} r_1^2, \text{ for all } i = 1,2,3,4\ldots \tag{6}$$

Four unknowns $(x, y, z, \text{and } r_1)$ are represented by Eq. (6). Thus, a minimum of four detector positions are required to determine these unknowns. Note that k_{1i} is evaluated by the intensities at the first and the i^{th} detector positions. The set of four equations represented by Eq. (6) (for $i = 1,2,3,4$) are non-linear and can be solved for four unknowns if all the detector positions (x_i, y_i, z_i) and the constants k_{1i} are known. The quadratic nature of the problem forces it to have two solutions—one of which is the real source position. This ambiguity is similar to one presented in [5] and can be avoided by incorporating one more detector position. The solution that best satisfies the fifth detector equation (for $i = 5$ in Eq. (6)) is deemed the predicted source position. Therefore, information of intensities at no fewer than five different detector positions is essential for localization through the proposed algorithm.

The approach to localization utilizes a domain discretization scheme. This scheme works by adaptively meshing the source domain into a finite number of discrete cells (see Figures 2.1 and 2.2) and utilizing statistic-based successive refinements for convergence. For the convergence criterion, the standard deviation σ of the $I_i r_i^2$ values is minimized. Theoretically—with no statistical variation and detection uncertainties—centroids of cells near the actual source position should better satisfy the inverse-square relationship. At the actual source position, $I_i r_i^2$ is constant which implies the variance σ^2 and standard deviation σ of the $I_i r_i^2$ quantities would theoretically be zero.

$$\sigma = Std(I_1 r_1^2, I_2 r_2^2, \ldots, I_n r_n^2) \tag{7}$$

In real-time detection, $I_i r_i^2$ is not necessarily constant since I_i is subject to statistical fluctuations together with finite dead-time of the detection system, and the attenuation and scattering of photons by the intervening medium. In this case, σ is expected to approach zero; hence its minimization.

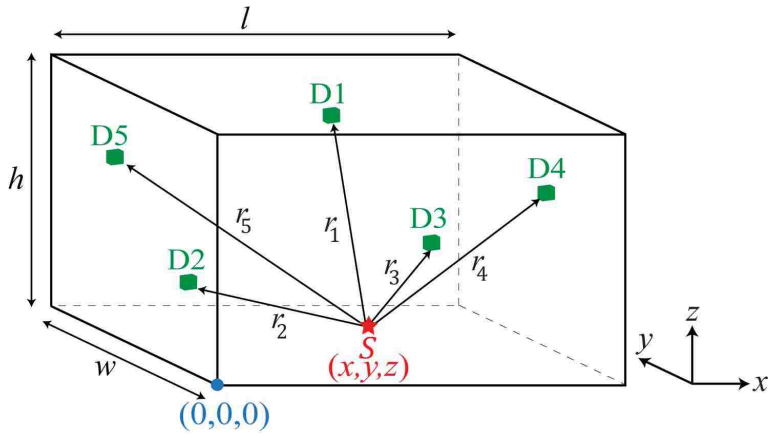

Figure 2.1 A representation of the domain in which the source is backtraced ($n = 5$).

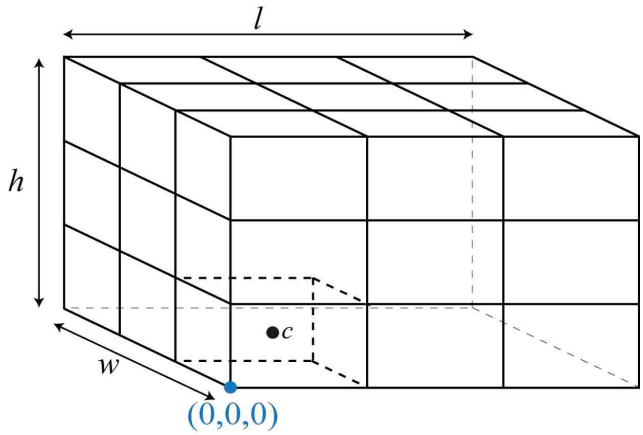

Figure 2.2 Domain discretization: The centroid of the discrete cell is represented by c ($N = 3$).

2.1. RADIATION SOURCE LOCALIZATION IN A REAL-TIME SCENARIO

Consider that the source domain has dimensions $l \times w \times h$ such that it encompasses both the source and n different detector positions. The domain is discretized into $N \times N \times N$ cells (see Figures 2.1 and 2.2). Assume the origin to be at a corner of the domain, the centroid of the m^{th} cell, (x_{cm}, y_{cm}, z_{cm}), can be determined—since l, w, h, and N are all known. The distance between the centroid and the i^{th} detector position (x_i, y_i, z_i), r_{mi}, can be calculated using Eq. (4):

$$(x_{cm} - x_i)^2 + (y_{cm} - y_i)^2 + (z_{cm} - z_i)^2 = r_{mi}^2 \tag{8}$$

The radiation intensity (I_i) represents the counts at i^{th} detector position, for a particular measurement time. The standard deviation $_{(m,0)}$ at the onset of iteration for the m^{th} cell is

$$\sigma_{m,0} = Std(I_1 r_{m1}^2, I_2 r_{m2}^2, \ldots, I_n r_{mn}^2) \tag{9}$$

Therefore, each of the N^3 cells will have its respective $\sigma_{(m,0)}$ value. Twenty cells with the smallest values of $\sigma_{(m,0)}$ are selected from these N^3 cells. Both the x_{cm}, y_{cm}, z_{cm} coordinates of the centroids and the $\sigma_{(m,0)}$ values of the selected cells are stored in a 20×4 matrix L_0, where the fourth column stores their respective $\sigma_{(m,0)}$ values. Each of these twenty cells is further discretized into smaller $N \times N \times N$ cells, and twenty cells with the smallest $\sigma_{(m,1)}$ values are selected for each cell. This process results in a total of 20^2 cells from which twenty cells with the smallest values of $\sigma_{(m,1)}$ are selected in the first iteration. A matrix $\boldsymbol{L_1}$ containing these selected cells is created as $\boldsymbol{L_0}$ was created. The discretization and evaluation processes are repeated until the k^{th} iteration, which satisfies:

$$\boldsymbol{L}(:,4)_{k^{th}} - \boldsymbol{L}(:,4)_{(k-1)^{th}} = \boldsymbol{0} \tag{10}$$

The process flow is provided in Figure 2.3. The twenty positions defined in the $\boldsymbol{L}_{k^{th}}$ matrix are the positions that best satisfy the inverse-square law. Thus they should be the best candidates for the actual source position. This scheme was successfully developed and implemented in MATLAB.

2.2. COMPUTATIONAL EFFICIENCY AND CONVERGENCE OF THE METHOD

Statistic-based grid-refinement method is the basis of algorithm described in the preceding section. Grid based methods are known to be computationally expensive (see Figure 2.4(a) for grid number basis vs. computational time). By choosing low value of N, implementation of the successive grid refinement eliminates large portions of the domain quickly, resulting in relatively fast computational time. Statistic-based refinement methods may provide convergence issues. A rudimentary test of convergence was performed by testing the method on 341 source positions in the domain. The domain was divided in to $5 \times 5 \times 5$ cubes; MCNP simulation was performed for 125 centroids and 216 corners of

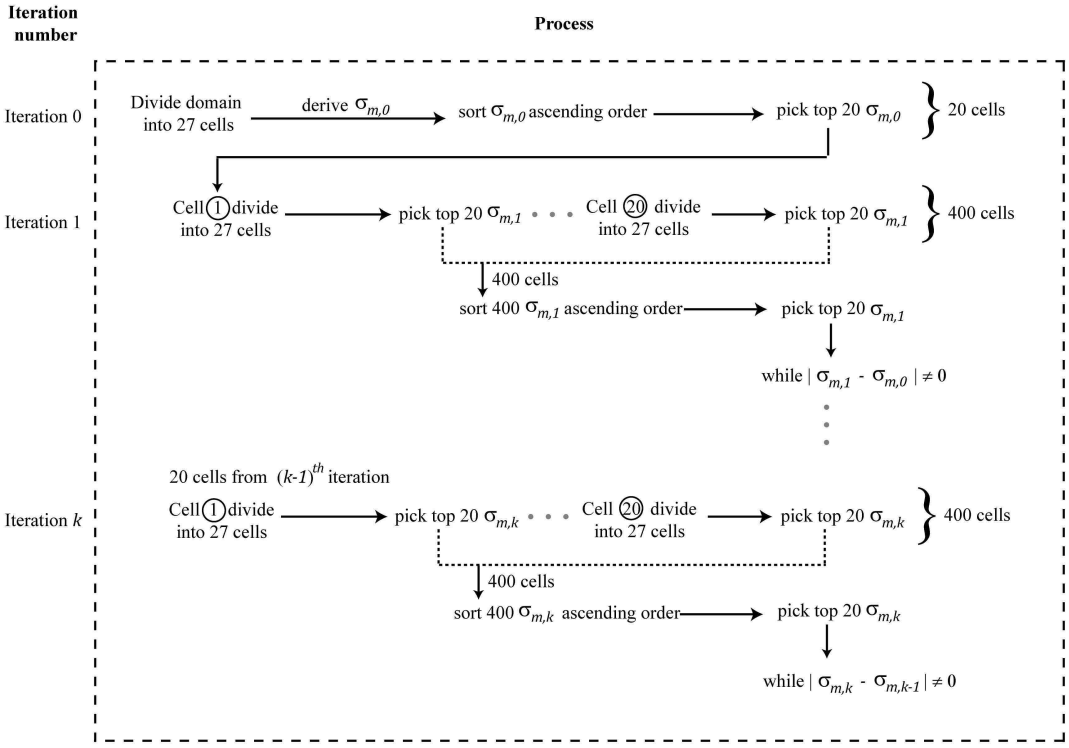

Figure 2.3 Statistic-based grid-refinement method process flow ($N = 3$).

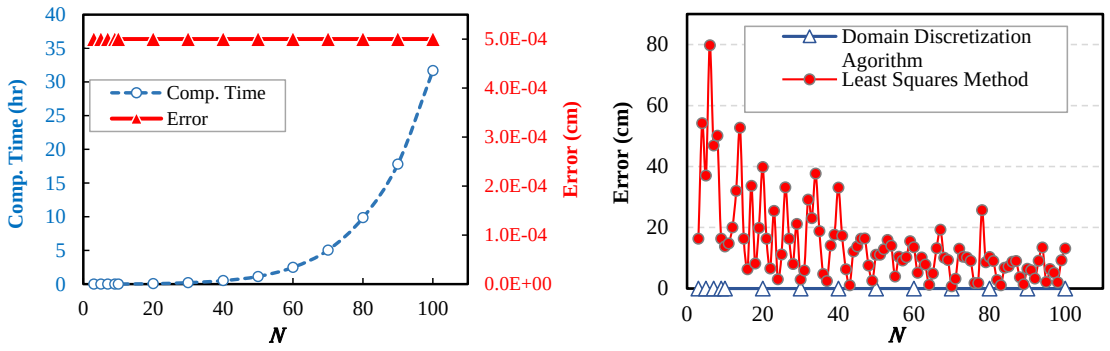

Figure 2.4 Results for the MCNP simulation presented in the Section 3. Variation of error with N for (a) domain discretization algorithm and (b) least squares method [13]. Respective computation times for domain discretization algorithm is also shown in (a). Error is defined as the distance between estimated and the actual source position.

the cubes and the algorithm was applied to backtrace the source and it converged in each case. Thus the statistic-based grid-refinement method appeared to overcome computational efficiency and convergence limitations.

3. VERIFICATION OF BACKTRACING SCHEME

The motive behind simulation studies was to ensure that the error imposed by the algorithm in source localization was negligible. For this reason, an MCNP model of ideal case of a point source in non-attenuating medium was developed. This case is similar to an absolutely efficient detection system with no dead-time and statistical fluctuations such that the inverse-square law is perfectly satisfied. An MCNP simulation was performed by assuming a ^{137}Cs source at the position (238.8, 75.3, 74.6) cm. The obtained point-detector fluxes, at different detector positions, are given in Table 3.1. The statistical uncertainties in all of these fluxes were 0.12%. The distance between any detector pair was between 0.17 m and 1.15 m. These fluxes and the detector positions were used to predict the source position through the developed algorithm.

The algorithm used a domain discretization scheme, with $l = w = h = 500$ cm and $N = 3$, to localize the source (as described in subsection 2.1). Using the first five detector positions, the algorithm estimated the source position with an accuracy of 5 μm. This distance indicated that the error introduced by the backtracing scheme was negligible. The computation time of the MATLAB program was 2.85 seconds on a computer with a 2.20 GHz Intel Core2 Duo processor and a 2.0 GB installed RAM. Additional tests were performed for various values of N^3 cells. The computational time increased as N increased with no appreciable improvement in error (see Table 3.2 and Figure 2.4(a)). Thus, the computational efficiency of $3 \times 3 \times 3$ domain discretization was the motivation of choosing $N = 3$ for experimental validation.

3.1. COMPARISON WITH LEAST SQUARES METHOD

The results from MCNP simulation were also compared with the least squares method for different values of N. The approach presented in [13] (also discussed in [12]) was implemented using MATLAB and the same domain (with $l = w = h = 500$ cm) was discretized into $N \times N \times N$ cells. The centroid of the cell that minimized the sum of squared

errors was deemed the estimated source position. As stated in [12, 13], this method is computationally expensive particularly for higher values of N. In contrast, a higher value of N is desired for better source approximation. Thus, the least squares method was executed through quad-core parallel computing using MATLAB on a 2.67 GHz Core2 Quad CPU with 8.0 GB installed RAM. The error in source prediction from domain discretization algorithm and least squares method are compared in Figure 2.4(b). The error from least squares method dropped to approximately 10 cm at $N = 50$ and it did not significantly vary thereafter. Hence, $N = 50$ was chosen for experimental results using the least squares method. It is worth noting that the domain discretization scheme provided a considerably better accuracy of 5 μm for any value of N (see Figure 2.4(b)).

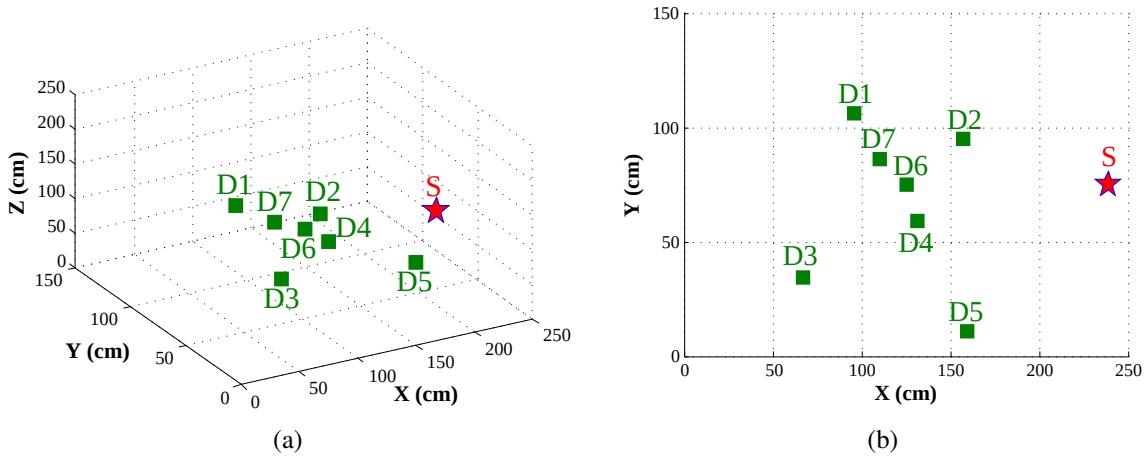

Figure 3.1 Expanded view of different detector positions and source placement: (a) 3D view and (b) XY view. Detector positions are indicated by green squares and the source position is indicated by the red star.

Table 3.1 Actual source and detector position coordinates and point-fluxes at different detector positions.

	x (cm)	y (cm)	z (cm)	Distance between source and detector position (cm)	Simulation: Point flux ($*10^{-7}$)
S	238.8	75.3	74.6	–	–
D1	95.6	106.0	102.2	149.0	8.95
D2	157.0	94.9	80.6	84.3	27.97
D3	67.0	34.6	88.3	177.0	6.34
D4	131.1	59.4	90.2	109.9	16.46
D5	159.4	10.8	104.8	106.6	17.49
D6	125.7	75.2	92.1	114.4	15.20
D7	109.9	86.4	96.5	131.2	11.55

Table 3.2 Variation in computation time as N increased.

N	N^3	Computation time (sec)	Error (μm)
3	27	2.85	5
5	125	6.91	5
7	343	14.46	5
9	729	28.83	5

4. VALIDATION BY EXPERIMENT

An experimental validation was performed subsequent to the verification of the backtracing scheme. The experimental setup mirrored the MCNP simulation but with real limitation like statistical fluctuations, background effect, and the impact of detector/detector conditions. A ^{137}Cs source of approximate activity 5.1 μCi was placed tabletop at the same position as that in the simulation studies. Canberra's NaI(Tl) scintillation detectors (Model: 802-2$\times$2, [14, 15]) with a photomultiplier tube base preamplifier [16] were used to record counts at the detector positions given in Table 3.1. At each position, one measurement was taken in the presence of source at successive intervals of one second. The background counts—taken one time for the same intervals in the absence of the source—were subtracted from these counts to obtain the net counts. A single measurement was important so that the influence of limited statistics—which is generally the case in real-time situations—could not be avoided. The experiment used 2048 channels of Lynx multi-channel analyzer (MCA) for spectrum analysis [17]. Averaged net counts collected at each detector position, obtained for the ^{137}Cs peak in the energy spectrum, were used in validation of the localization algorithm. Both the radiation source and the detectors were static during the experiment.

Figure 4.1 shows the plot of error—i.e. the distance between the estimated and the actual source position—with measurement time. The behavior of error was significantly erratic for $T < 2$ minutes. This observation seems reasonable since the weak nature of the source degrades the signal-to-noise ratio (SNR) leading to poor estimates at short measurement times. As an example, for initial periods of time, the contribution of the background counts at detector position D1 was greater than 60% of the total counts in the energy range of interest. As the time increased, however, the error dropped to approximately 40 cm (at $T = 4$ minutes). After $T = 7.3$ minutes, the error further dropped down and attained a fairly constant value of approximately 25 cm. Ideally, the error should decrease monotonically

as the measurement time increases. However, it showed an erratic behavior at various instances (see Figure 4.1). This observation was attributed to detection uncertainties. Also, the counts were taken for one single measurement.

To observe the impact of incorporating additional detector positions on source estimation, two more known detector positions—D6 and D7—were utilized. The variation of error for six and seven detector positions provided no significant improvement (see Figures 4.1(b)-(c). The general trend of the error with time was also maintained for these cases. Figure 4.1 also compares these results with the least squares method. The (erratic) behavior of the error from domain discretization algorithm is comparable to the least squares method using the same set of measurement data.

Figure 4.2(a) illustrates the variation of error in each direction (x, y, and z) with the measurement time, for five, six, and seven detector positions. The error in each direction is defined as the absolute difference between the estimated coordinate and the actual coordinate in that direction. For example, in x direction, $E_x = |x_{estimated} - x_{actual}|$. Estimations of x and y coordinates were relatively closer to the actual x and y coordinates of the source position. The error behavior in x and y directions was significantly erratic for $T <$ 2 minutes. The error in these directions dropped after 3 minutes of measurement time and tended to approach zero as the measurement time increased. This was true for all cases (Figure 4.2). The main contribution to the (total) error was from the estimated position's z-component. Therefore, the trend of the total error mimicked the error in the z-direction. Relatively poor estimates in the z-direction were attributed to the fact that there was no significant variation in the z-coordinates of different detector positions (see Table 3.1). The detector positions covered approximately 92 cm and 95 cm variation in the x and y directions, respectively. However, the positions covered just 24 cm in the z-direction. The error in z direction would likely be reduced as the additional detector positions, having significant variation in z-direction, are incorporated in the algorithm. The dependence of source

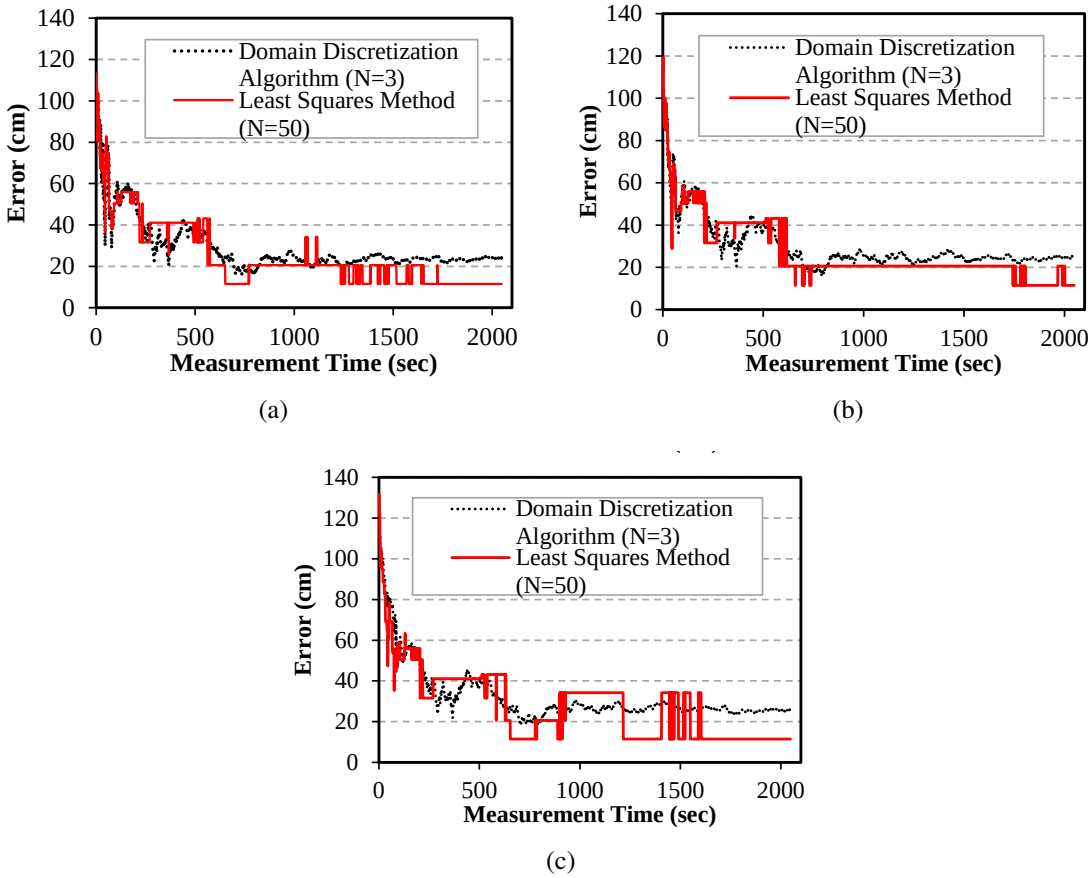

Figure 4.1 Experimental results: error comparison with least squares method [12, 13] for (a) five, (b) six, and (c) seven detector positions.

localization on detector position is being considered as a topic for additional work in this area.

The average computation time taken by the MATLAB on a 2.20 GHz Intel Core2 Duo processor with 2.0 GB installed RAM, for different cases is given in Table 4.1. The algorithm was computationally efficient even with additional detector positions. The computational efficiency of the discretization scheme, implemented using MATLAB, justified the deployment of this algorithm in real-time scenarios. The computational time for least squares method, however, was considerably larger and it increased with additional detector positions.

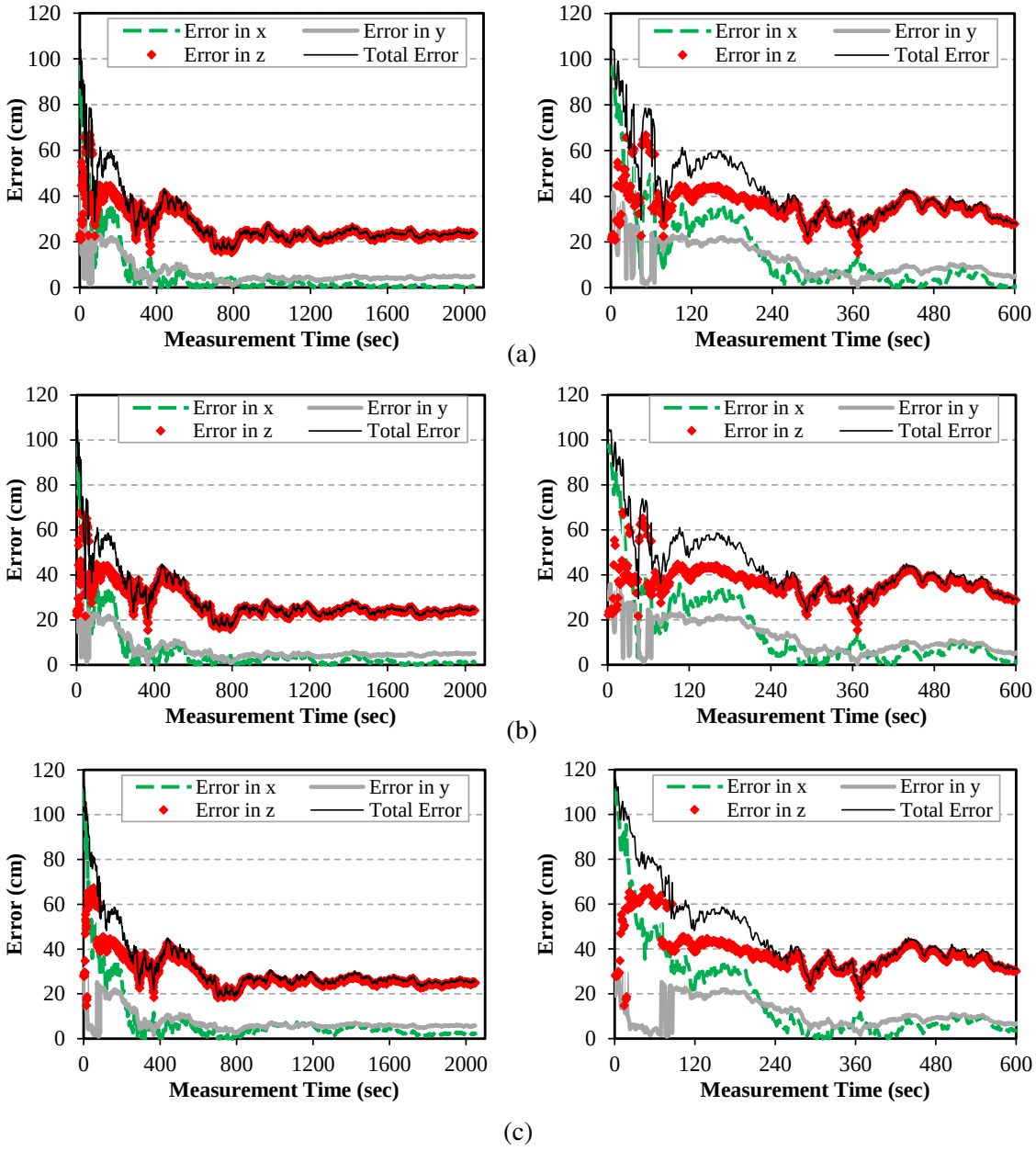

Figure 4.2 Experimental results using domain discretization algorithm: error in x, y, and z directions with measurement time. Error based on first (a) five, (b) six, and (c) detector positions with its zoomed plot on the right.

It is believed that the measurement time needed to localize the sources should decrease with stronger sources (as used in [3, 12, 18]). The experiment showed that the counts registered in approximately 2-3 minutes of measurement time were sufficient to localize the source with reasonable accuracy (< 60 cm). The equivalent activity that will register same

counts in 1 second of measurement time will therefore be 0.61-0.92 mCi. Therefore, for the same physical placement of source and detectors, it is expected that a source of approximate activity 0.61-0.92 mCi will be localized in approximately one second of measurement time.

Table 4.1 Average number of iterations and computational time for different detector positions.

Detector Positions	**Domain discretization algorithm**		**Least squares method [12, 13]**
	Average number of iterations	**Average computational time for $N = 3$ (s)***	**Average computational time for $N = 50$ (s)†**
D1-D5	35.8	2.70	5.43
D1-D6	35.2	2.72	6.02
D1-D7	35.3	2.76	6.63

*On a 2.20 GHz Intel Core2 Duo processor with 2.0 GB installed RAM.

†When using quad-core parallel computing in MATLAB on a 2.67 GHz Core2 Quad CPU with 8.0 GB installed RAM.

5. CONCLUSION

This work describes an approach that can be used to localize the source in a three-dimensional domain. An algorithm was developed and implemented using MATLAB and uses a domain discretization scheme to predict the source position using measurements from different detector positions.

Results of simulation and experimental studies are presented for a ^{137}Cs source. The simulation results indicate that a 100% efficient detection system with zero dead-time introduced a near zero error in localization. In experimental validation with a weak ^{137}Cs source of strength 5.1 μCi and five detector positions, a reasonable accuracy of approximately 53 cm was achieved. The prediction improved and stabilized to approximately 25 cm for higher measurement times. The additional detector positions, however, provided no significant improvement in the source prediction. The difference in between the predicted source position and ground truth was primarily due to error in the prediction of the source's elevation. The results are also compared with the least squares method. The (erratic) behavior of the error from domain discretization scheme is comparable to the least squares method. An excellent prediction in simulation results, combined with a reasonably accurate prediction in experimental results, indicated that errors in source localization were primarily due to detection uncertainties. For a typical detection system, the line of sight between the source and the detector, detector efficiency, and system dead-time play a significant role in quantifying the source intensity at the detection position. These system parameters must be known in order to properly quantify the intensity (I_i). The impact was evident in the experiment results such that the errors obtained were exclusively due to detection parameters: measurement time, efficiency, dead-time, and line of sight. The better the sensitivity of a detection system, the better consistency in $I_i r_i^2$ values at all detector positions is expected. Hence, a better estimation of the source position could be achieved. The computation time on a 2.20 GHz Intel Core2 Duo processor with 2.0 GB RAM was within the range of 2.7

and 2.85 seconds even when additional detector positions were used. The viability of deploying this scheme in real-time applications is predicated by its computational efficiency. It is expected that a radioactive source of approximate activity 0.61-0.92 mCi can be localized in real-time with a measurement time of approximately 1 second, for same physical placement of source and detectors. Moreover, the localization of multiple sources with different energy signatures is possible when a detection system, coupled with a multi-channel analyzer, is used.

ACKNOWLEDGEMENTS

The work presented in this paper is supported by U.S. NRC under the Award Number NRC-HQ-11-G-38-0008.

REFERENCES

[1] N.S.V. Rao, M. Shankar, J.C. Chin, and D.K.Y. Yau. Identification of low-level point radiation sources using a sensor network. *ACM Transactions on Sensor networks*, 7(3), 2010.

[2] J.W. Howse, L.O. Ticknor, and K.R. Muske. Least squares estimation techniques for position tracking of radioactive sources. *Automatica*, 37(11):1727–1737, 2001.

[3] R. Vilim and R. Klann. Radtrac: A system for detecting, localizing, and tracking radioactive sources in real time. *Nuclear Technology*, 168(1):61, 2009.

[4] J.C. Chin, D.K.Y. Yau, N.S.V. Rao, Y. Yang, C.Y.T. Ma, and M. Shankar. Accurate localization of low-level radioactive source under noise and measurement errors. *Computer Science Technical Reports, Paper 1700*, 2008. URL `http://docs.lib.purdue.edu/cstech/1700`. Accessed February 23, 2015.

[5] J. Cox and M.B. Partensky. Spatial localization problem and the circle of apollonius. *arXiv preprint physics/0701146*, 2007.

[6] N.S.V. Rao, S. Sen, N.J Prins, D.A. Cooper, R.J. Ledoux, J.B. Costales, K. Kamieniecki, S.E. Korbly, J.K. Thompson, J. Batcheler, R. R. Brooks, and C.Q. Wu. Network algorithms for detection of radiation sources. *Nuclear Instruments and Methods in Physics Research Section A: Accelerators, Spectrometers, Detectors and Associated Equipment*, 784:326–331, 2015.

[7] X. Xu, N.S.V. Rao, and S. Sahni. A computational geometry method for localization using differences of distances. *ACM Transactions on Sensor Networks (TOSN)*, 6(2): 10, 2010.

[8] N.S.V. Rao. Identification of simple product-form plumes using networks of sensors with random errors. In *Proceedings of the 9th International Conference on Information Fusion,*, pages 1–8. IEEE, 2006.

[9] G. Mellen, M. Pachter, and J. Raquet. Closed-form solution for determining emitter location using time difference of arrival measurements. *Aerospace and Electronic Systems, IEEE Transactions on*, 39(3):1056–1058, 2003.

[10] H.C. Schau and A.Z. Robinson. Passive source localization employing intersecting spherical surfaces from time-of-arrival differences. *Acoustics, Speech and Signal Processing, IEEE Transactions on*, 35(8):1223–1225, 1987.

[11] N.S.V. Rao, M. Shankar, J.-C. Chin, D.K.Y. Yau, Y. Yang, X. Xu J.C. Hou, and S. Sahni. Localization under random measurements with application to radiation sources. In *Proceedings of the 11th International Conference on Information Fusion*, pages 1–8. IEEE, 2008.

[12] A. Gunatilaka, B. Ristic, and R. Gailis. Radiological source localisation. 2007. URL http://www.dtic.mil/cgi-bin/GetTRDoc?AD=ADA471550. Accessed July 2, 2013.

[13] I. Takumi, M. Nagai, S. Kato, M. Hata, and H. Yasukawa. Estimation of EM source location from 223 Hz EM field power data at multiple spots. In *Geoscience and Remote Sensing Symposium, 2001 (IGARSS'01). IEEE 2001 International*, volume 7, pages 3191–3193. IEEE, 2001.

[14] *Model 802 Scintillation Detectors*. Canberra Industries. URL http://www.canberra.com/products/detectors/pdf/Model-802-SS-CSP0232.pdf. Accessed July 2, 2013.

[15] S.A. Dewji. Assessing internal contamination after a radiological dispersion device event using a 2×2-inch sodium-iodide detector. Master's thesis, Georgia Institute of Technology, 2009. URL https://smartech.gatech.edu/xmlui/bitstream/handle/1853/28092/dewji_shaheen_a_200905_mast.pdf. Accessed July 2, 2013.

[16] *Model 2007/2007P Photomultiplier Tube Base/Preamplifier*, . URL http://www.canberra.ru/html/products/detectors/preamplifiers/2007p.pdf. Accessed July 2, 2013.

[17] *Lynx Digital Signal Analyzer*, . URL http://www.canberra.com/fr/produits/radiochemistry_lab/pdf/Lynx-SS-C38658.pdf. Accessed Oct. 24, 2015.

[18] M. Chandy, C. Pilotto, and R. McLean. Networked sensing systems for detecting people carrying radioactive material. In *Proceedings of INSS 2008 - 5th International Conference on Networked Sensing Systems*, pages 148–155. IEEE, 2008.

II. MCNP MODELING OF A NEUTRON GENERATOR AND ITS SHIELDING AT MISSOURI UNIVERSITY OF SCIENCE AND TECHNOLOGY

Manish K. Sharma, Ayodeji B. Alajo, Xin Liu

Missouri University of Science & Technology,

Nuclear Engineering, Rolla, MO, USA

ABSTRACT[‡]

The shielding of a neutron generator producing fast neutrons should be sufficient to limit the dose rates to the prescribed values. A deuterium-deuterium neutron generator has been installed in the Nuclear Engineering Department at Missouri University of Science and Technology (Missouri S&T). The generator produces fast neutrons with an approximate energy of 2.5 MeV. The generator is currently shielded with different materials like lead, high-density polyethylene, and borated polyethylene. An MCNP transport simulation has been performed to estimate the dose rates at various places in and around the facility. The simulations incorporated the geometric and composition information of these shielding materials to determine neutron and photon dose rates at three central planes passing through the neutron source. Neutron and photon dose rate contour plots at these planes were provided using a MATLAB program. Furthermore, the maximum dose rates in the vicinity of

[‡]Published in Nuclear Instruments and Methods in Physics Research Section A (2014).

the facility were used to estimate the annual limit for the generator's hours of operation. A successful operation of this generator will provide a convenient neutron source for basic and applied research at the Nuclear Engineering Department of Missouri S&T.

Keywords: Neutron generator shielding, D-D neutron generator, MCNP, Dose

1. INTRODUCTION

Recently, a deuterium-deuterium (D-D) neutron generator (model DD-109), manufactured by Adelphi Technology, was installed in the Nuclear Engineering (NE) Department at Missouri University of Science and Technology (Missouri S&T). The generator utilizes D-D fusion reactions to produce fast neutrons. The positively charged deuterium ions, generated from the plasma ion source, are accelerated and bombarded on the target by using a high electric field. The target is negatively biased to "attract" these positively charged deuterium ions. A beam current of about 5 mA-15 mA, with an accelerating potential in the range of 80 kV and 120 kV, is maintained to establish this high electric field. The accelerated D+ ions strike a static 1.02 cm thick V-shaped copper target with a titanium coating of approximate thickness of 0.102 mm. During the initial period of time, the impinging D+ ions form titanium hydride on the surface of the target. Subsequent bombardment of D+ ions results in the production of fast neutrons with an approximate energy of 2.5 MeV through $^{2}H + {}^{2}H \rightarrow {}^{3}He + n$ fusion reactions [1–3]. Figure 1.1 shows the DD-109 generator head, the high-density polyethylene (HDPE) blocks used in its shielding, and the V-shaped target where the fast neutrons are produced. In the DD-109 neutron generator installed at Missouri S&T, the target is oriented such that the open side of a V-shaped target faces up where the samples will be placed (see Figure 1.1(b)).

Bombardment of D+ ions also results in deposition of heat at the target. The target, therefore, has channels with fluorinert running through them. The fluorinert is specifically needed to cool the high voltage part (target) of the generator. However, the microwave plasma section (including the magnetron power supply in the rack) is cooled with water. The detailed working mechanism of the neutron generators, utilizing deuterium-deuterium and deuterium-tritium fusion reactions and their applications, has been thoroughly discussed in the literature [1–5].

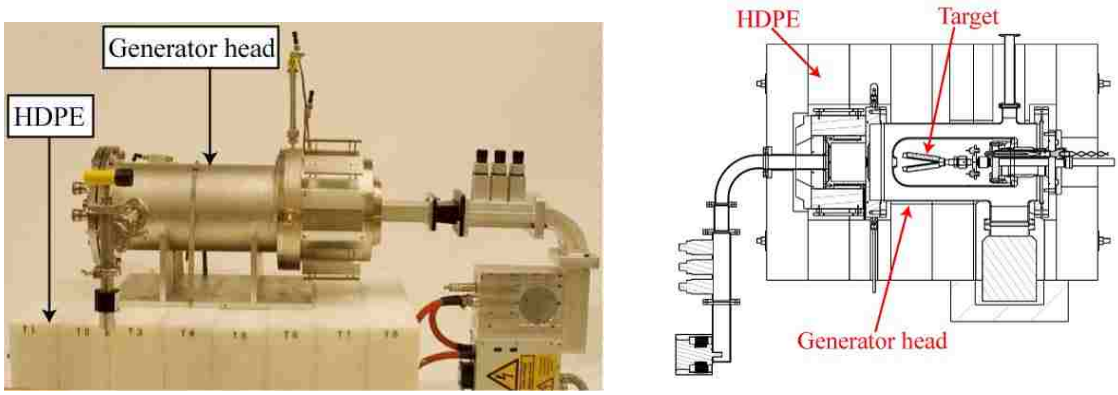

(a) (b)

Figure 1.1 (a) DD-109 generator and HDPE blocks used in shielding and (b) cutaway of neutron generator and surrounding HDPE shielding. V-shaped target of the generator (top view) is also shown (Image courtesy of Adelphi Technology, Inc.).

The operation of this DD-109 neutron generator at Missouri S&T will provide faculties and students a convenient neutron source that can be used for various basic and applied research efforts, such as neutron activation, radiography, and material irradiation, etc. Since the neutron generator is installed in a room in a campus building (see Figure 1.2), it is imperative that appropriate radiation shielding be provided to protect the public and operators of the generator from radiation exposure. It is very well known that the shielding of neutrons is a complicated problem due to the fact that both neutron and photon interactions with matter should be considered. Therefore, for sufficient reduction in neutron and photon dose rates, the generator has been shielded with high-density polyethylene, lead, and borated polyethylene (BPE). In addition, some walls of the generator room were lead-lined to limit the dose rates to the operator and the public.

In the past, various studies have been performed to design shielding for different neutron sources and generators. The MCNP [6] modeling of a deuterium-tritium (D-T) neutron generator was well studied by J. Katalenich et al. [7]. The yield of uncollided 14.1 MeV neutrons from the D-T neutron reactions, and the neutron fluxes for different

beam port diameters, were estimated in this work. J.C. Liu et al. [8] discussed the optimal shielding design for a 14 MeV D-T neutron generator using the MCNP4B radiation transport code. The effectiveness of various materials and geometries in shielding the D-T generator were examined in this study. A thorough analysis of the shield design of a D-T neutron generator was also performed by D.L. Chichester et al. [9]. In their work, Monte Carlo simulations were performed to determine the effectiveness of the concrete shield in reducing the dose rates due to D-T neutron generators. The independent neutron and photon dose rates, due to 14.1 MeV neutron source terms at three different locations, were determined at various positions around the facility. The results from the MCNP5 radiation transport code and SCALE5 code were compared and discussed. The analytical calculations and Monte Carlo simulations for the design of shield walls for different neutron sources were performed by D.L. Chichester et al. [10]. The spatial profile of dose rates, due to the ^{252}Cf spontaneous fission neutron source and neutrons from D-T fusion neutron generators, were obtained at horizontal and vertical planes. The MCNP5 radiation transport code was utilized in simulating the neutron and photon radiation fields in the facility. The effectiveness of different shielding materials in reducing the neutron and photon dose rates has been discussed in [11]. The MCNP simulations were performed by assuming a point-like isotropic source emitting 1 x 10^8 neutrons/s of energy 14.1 MeV.

In this work, attempts were made to model the current radiation shielding of the D-D neutron generator and the installation room using MCNP. The ultimate goal of this study was to estimate the approximate dose rates in and around the facility where the generator will be operated, and to determine the maximum operation time of the generator so that the annual radiation doses to the operator and the public would be within the prescribed limits. Furthermore, an additional MCNP transport simulation, without the lead-lining of different walls and floor, was performed. The purpose of this simulation was to estimate the shielding effectiveness of lead-lining in reducing the neutron and photon dose rates.

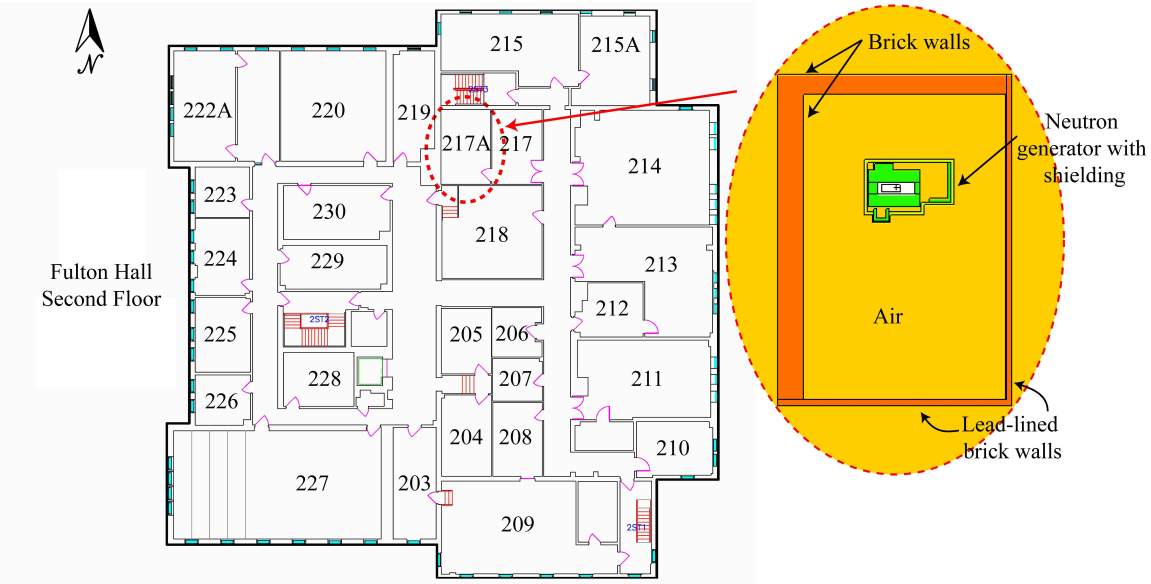

Figure 1.2 Layout of second floor of the Fulton building where the generator is located. Also shown is a zoomed image of the room (217A) where the generator is installed.

2. FACILITY LAYOUT AND ANALYTICAL CALCULATIONS

It was discussed in the previous section that, for successful operation of the neutron generator, sufficient shielding should be provided to minimize exposures to the operating personnel and public within the prescribed limits. This section describes the layout of the facility and the details of different materials used in shielding the neutron generator. Some analytical calculations were also performed to theoretically estimate the exposure rates due to the neutron source.

Figure 1.2 shows the layout of the second floor of the Fulton building on the Missouri S&T campus where the DD-109 generator is currently installed. The generator is located in room 217A on this floor and can be controlled through a computer system located in the adjoining room (room 217 in Figure 1.2).

The operation of the neutron generator will produce high energy fast neutrons with an approximate energy of 2.5 MeV. For efficient thermalization of these fast neutrons, produced through D-D fusion reactions at the target, the generator head was first surrounded by high-density polyethylene (see Figure 1.1(b)). Elastic scattering of neutrons by hydrogen atoms in HDPE made it a suitable material for this purpose [12]. Thereafter, inclusion of material with a high atomic number was preferred for attenuating the secondary gamma photons produced. This strategic placement of low and high atomic number materials eventually helped to reduce the exposure due to gamma photons. Therefore, the HDPE that surrounded the neutron generator head was covered with a 0.64 cm (0.25 in.) thick lead box (see Figures 2.1 and 2.2). It is believed that the majority of gamma photons were produced by the neutron capture reaction $^{2}H(n,\gamma)^{2}H$, which released a 2.22 MeV gamma ray. One of the purposes of this study was to determine if the amount of lead, together with the walls of the generator room, were adequate for attenuating the gamma rays.

Additionally, this whole configuration was covered with 5.08 cm (2 in.) thick 5% wt. borated polyethylene to absorb the thermalized neutrons (see Figures 2.1 and 2.2). It

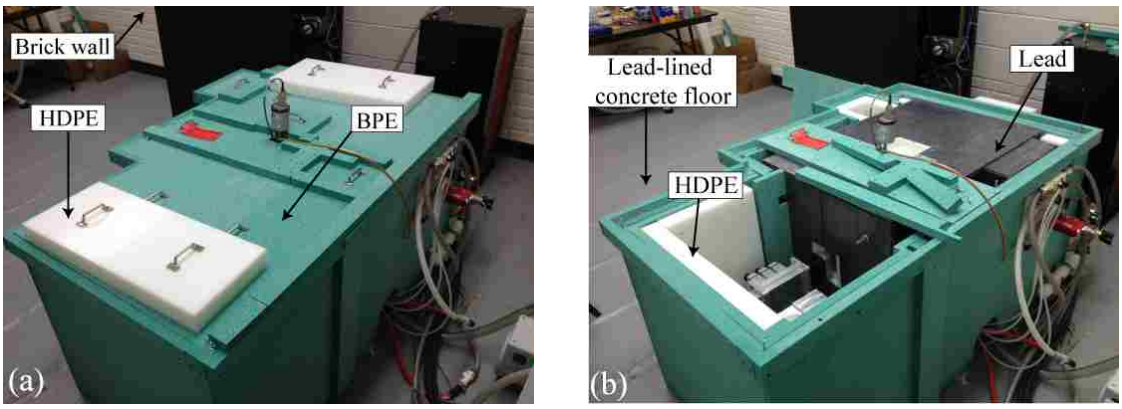

(a) (b)

Figure 2.1 The DD-109 neutron generator with (a) current shielding and (b) the inside of the top borated shielding. The place where samples will be irradiated is also shown.

should be noted that the shielding for the neutron generator was provided by the manufacturer of the generator (Adelphi Technology). The shape of the shielding was chosen to "form fit" the generator while utilizing the rectangular pieces of polyethylene (see Figure 2.2). This design will also provide more open space for accessing the place where the samples will be irradiated (see Figure 2.1(b)). Therefore, in this study, attempts were made to determine the effectiveness of the shielding (provided by the manufacturer) and to estimate the limit on the annual hours of operation of the generator if it was operated with the current shielding.

To further reduce the dose rates, the walls of the generator room were provided with additional shielding materials. The east and the south walls are both made of brick 10.16 cm (4 in.) thick. To reduce the photon dose rate in the adjoining rooms (room 217 and 218 in Figure 1.2), the east and south walls were both lined with 0.32 cm (0.125 in.) thick lead on the inner side of the generator room (see Figures 2.1(a) and 3.2). The floor is made of 32.39 cm (12.75 in.) thick concrete and also has a 0.64 cm (0.25 in.) thick lead lining. This strategic lining of lead in the floor is to minimize the photon dose that would be received by persons working on the first floor of the building. The west and north walls of the generator room are made of 43.18 cm (17 in.) and 32.39 cm (12.75 in.) thick brick,

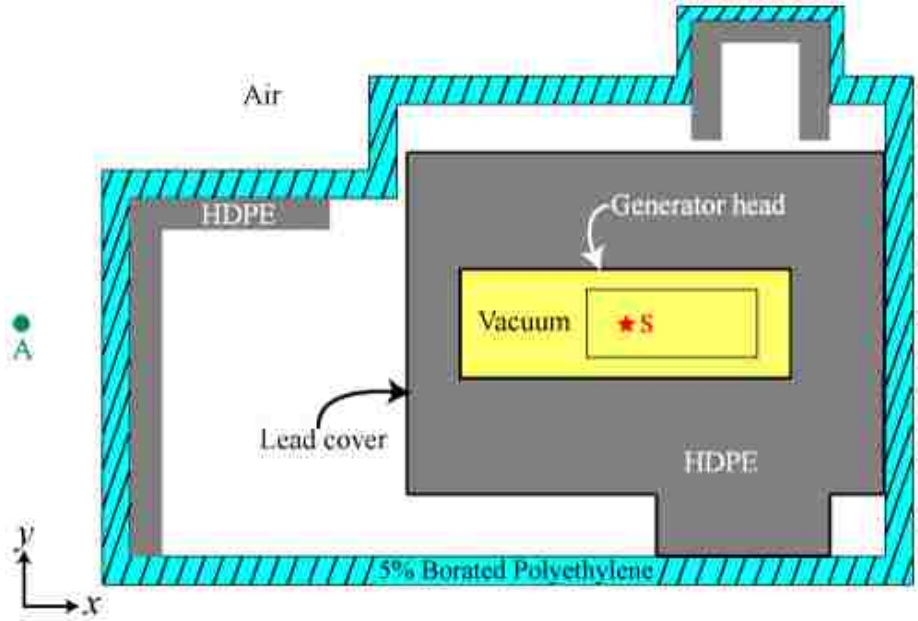

Figure 2.2 Scaled diagram of current shielding of neutron generator (central plane, *xy* view). The neutron source shown by a red star is assumed to be a point source at origin. Reference position A that was used in analytical calculations is also shown.

respectively (see Figures 1.2 and 3.1). The roof of the generator room has a 2.54 cm (1 in.) thick wood covering. Although, the roof is constructed of a composite single material after the wood covering, the simulations were performed by assuming attenuation from the wood covering only. This conservative assumption was made so that the reported dose rates would be an overestimation of the actual values. The definitions and compositions of different materials used in shielding the generator and the walls of the generator room are provided in Table2.1. As will be discussed in section 3, the geometric and composition details of the shielding and the walls of the generator room were used in developing the MCNP model for dose estimation at different planes.

2.1. ANALYTICAL CALCULATIONS

Analytical calculations were performed to theoretically estimate the neutron dose rate for a reference position (1 m away from the source). The idea was to understand the effectiveness of the shield and to compare the calculated dose rate (at a reference point) with

the dose rate obtained from MCNP simulations. NCRP Report No. 144 provided guidance for calculation of neutron dose rates for different thicknesses of concrete shielding [13]. This report also recommends the "removal cross-section" method for dose rate determination when neutrons of energy less than 30 MeV are shielded with hydrogenous materials. However, this method requires the information of buildup factor (which accounts for dose contribution due to scattered neutrons). Moreover, the buildup factor varies with the thickness of the shield [2]. Therefore, an alternative approach, recommended in [2], was used to approximate the dose rate at the reference position 1 m away from the source in the east direction (see position A in Figure 2.2):

$$DE_T = DE_0 * C * e^{-T/\lambda} \tag{1}$$

where DE_T and DE_0 are the dose equivalent values at a particular position with and without a shield of thickness T, λ is the relaxation length, and C is a constant which incorporates the scattering factor for correction. At position A in the east direction ($-x$ direction in Figure 2.2), the neutrons will encounter approximately 14.3 cm of HDPE and approximately 5.08 cm of BPE. Since lead is not a very effective material in reducing neutron dose rates [11], the attenuation offered by 0.64 cm (0.25 in.) thick lead box was ignored in our calculations. Moreover, the densities and the neutron removal cross sections of HDPE, BPE, and paraffin were approximately the same [12, 14]; therefore the relaxation length of paraffin provided in [2] was used for dose rate estimation at reference position A.

The unshielded dose rate at any point (DE_0 distant R cm away from a neutron source of strength S neutrons per second is given by

$$DE_0 = \frac{Sq}{4\pi R^2} \tag{2}$$

where q is the dose-equivalent rate per unit neutron fluence rate (in Svh^{-1} per neutron cm^{-2} s^{-1}, provided in [12]). For a neutron source emitting 2.5 MeV neutrons with a rate of 2

$\times$ 10^9 neutrons/s, the unshielded and shielded neutron dose rate, at reference position A, were calculated to be 22.25 mSv/h and 0.99 mSv/h, respectively. The shielding of the generator therefore reduced the neutron dose rate by an approximate factor of 22 (in the east direction). This observation highlighted the importance of incorporation of hydrogenated shielding materials for effective reduction of neutron dose rates. The analytical estimate of the neutron dose rate at the reference position (with shielding) was also found to be reasonably close to the dose rate value obtained for that position from the MCNP simulations: 1.11 mSv/h. Details of the MCNP model and simulations performed using the MCNP5 radiation transport code are given in section 3.

Table 2.1 Composition of different materials used in MCNP modeling of the generator head, its shielding, and the facility [15, 16].

Element	**Material (weight fraction)**								
	HDPE	**BPE**	**Lead**	**Brick (common silica)**	**Concrete (regular)**	**Wood**	**Air**	**Stainless Steel (304)**	**Aluminum (alloy 6061-O)**
Al				0.005	0.034				0.972
Ar							0.0128		
B		0.0469							
C	0.8563	0.7232				0.497	0.0001	0.0004	
Ca				0.014	0.044	0.002			
Cr								0.19	0.002
Cu									0.0028
Fe				0.007	0.014			0.7017	0.0041
H	0.1437	0.127			0.01	0.0596			
K						0.002			
Mg						0.002			0.01
Mn								0.01	0.0009
N						0.005	0.7553		
Na					0.029				
Ni								0.0925	
O		0.1029		0.525	0.532	0.4274	0.2318		
P								0.0002	
Pb			1						
S						0.005		0.0002	
Si				0.449	0.337			0.005	0.006
Ti									0.0009
Zn									0.0015
Density (g/cm^3)	0.93	0.937	11.35	1.8	2.3	0.64	0.0012	8	2.7

3. MCNP MODELING

As discussed in section 1, the target in the generator head has V-shape (see Figure 1.1). This target shape provided a larger surface area for the striking of D+ ions while still providing a relatively "small" source of neutrons. Therefore, in the MCNP modeling, an isotropic neutron point source of energy 2.5 MeV was assumed to be at the origin. This assumption was a conservative estimate because the attenuation offered by the target (and the fluorinert channels) was not accounted for in the model. The target was surrounded by an aluminum shroud that was approximately 0.15 cm (0.06 in.) thick and 12.7 cm (5 in.) in diameter. The shroud was surrounded by an outer wall which was made of 304 stainless steel of an approximate thickness of 0.28 cm (0.11 in.) and 20.32 cm (8 in.) in diameter. These geometric details of the generator head were provided by the manufacturer of the DD-109 neutron generator, Adelphi Technology Inc. It can be seen from the information provided by the manufacturer (see Figure 1.1) that it was reasonable to assume that the generator head was cylindrical in shape. This assumption was, therefore, used in the modeling of the generator head (see Figures 2.2 and 3.1).

The composition and properties of the materials in the generator head, shielding, and the walls of the generator room were either supplied by the manufacturer or taken from a compendium of material composition data. These are provided in Table 2.1 [15, 16]. The dimensional measurements, compositions, and densities of the generator head, shielding materials, and the facility (as discussed in section 2) were then incorporated in the final model. The *xy* and 3D views of the final model, as seen on the MCNPX visual plotter, are shown in Figure 3.1.

After the final model was developed, simulations were performed by assuming a maximum neutron yield of 2×10^9 n/s for the DD-109 generator and for a particle history of 1×10^9. The flux values, due to the isotropic point neutron source of 2.5 MeV energy at origin, were estimated for three planes passing through the source in each of the three

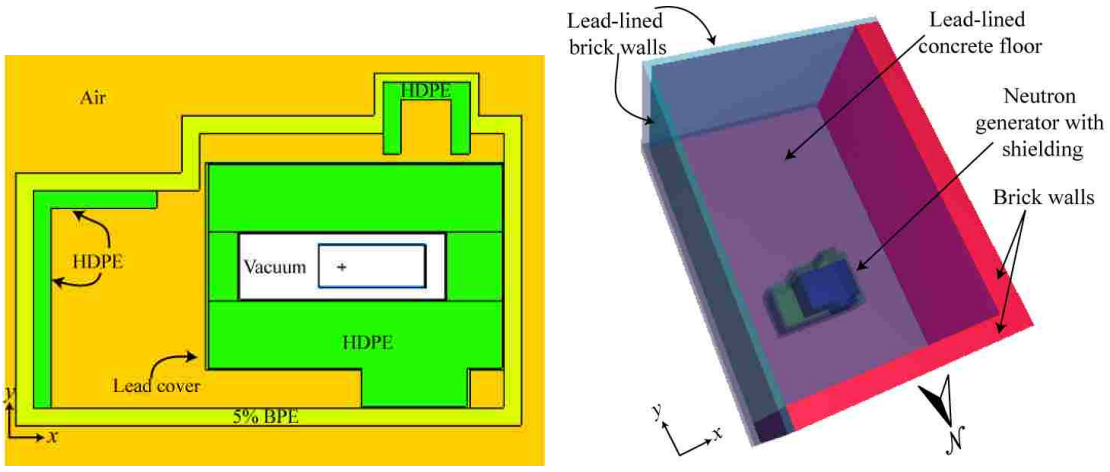

(a) (b)

Figure 3.1 Different views of the generator and its shielding, as seen on the MCNPX visual plotter (a) central plane, *xy* view (b) 3D view (roof of the room is not shown).

directions: x, y, and z (see Figure 3.2). These fluxes were obtained by creating a FMESH tally of 10 cm $\times$ 10 cm $\times$ 10 cm bins along these three central planes. The dose rates for three central planes, passing through the neutron source at origin, were then determined by using fluence-to-dose conversion factors for neutrons and photons based on ICRP publication 116 [17]. The neutron and photon dose rate contour plots (and their associated statistical uncertainties) for these central planes were generated using a developed MATLAB program. These dose rate contour plots were used to determine the maximum dose rates in the vicinity (six sides) of the generator room. The objective was to make a conservative estimate of the annual limit for operation time of this generator to keep the annual dose exposures within the prescribed values.

After estimation of the limit on annual operating hours of the neutron generator (with the current shielding), an additional simulation was performed to analyze the shielding effectiveness of lead-lining of east and south walls, and the concrete floor. The neutron and photon dose rates were simulated in the absence of lead-lining for same particle history of 1×10^9 (everything else was kept same in the MCNP model). The neutron and photon dose rates without the lead-lining were compared with the respective shielded dose

rate values at the same points just in the vicinity of each wall. The results are shown and discussed in the next section.

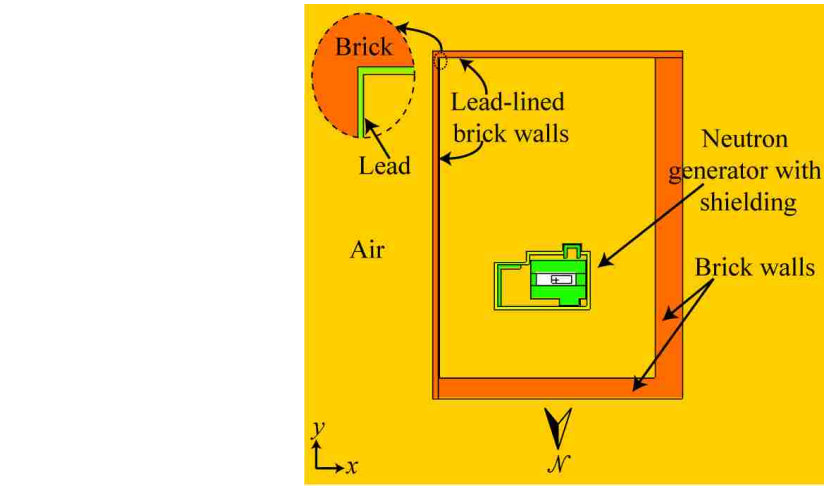

(a)

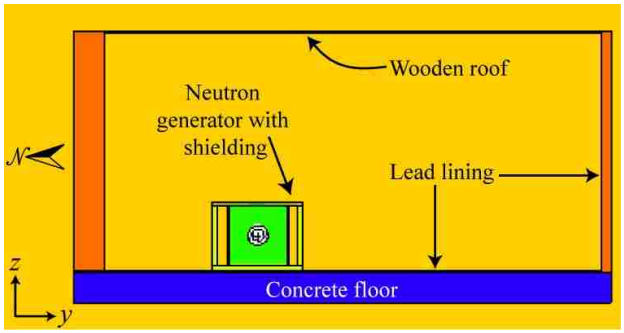

(b)

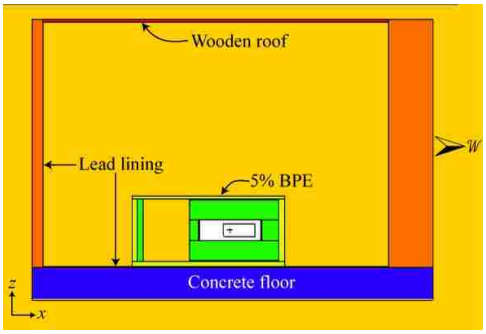

(c)

Figure 3.2 Central planes of the MCNP model where the dose rate contour plots were obtained. Figures were obtained using a MCNPX visual plotter for (a) *xy* view, (b) *yz* view, (c) *xz* view.

4. RESULTS AND DISCUSSION

As discussed in section 2 of this paper, the DD-109 generator head, its shielding, and the generator room were modeled using the MCNP5 radiation transport code. Simulations were then performed to determine the neutron and photon dose rates for three central planes as already explained in the previous section.

The dose rate contour plots (μSv/h) for three central planes, obtained using a developed MATLAB program, are shown in Figure 4.1. The respective statistical uncertainty associated with each dose rate is shown in Figure 4.2. These figures also illustrate the outer boundaries of generator shielding and of the facility to show the role of different materials in reducing the neutron and photon dose rates. For a better understanding of the distribution of dose rates in the facility, one can compare Figures 3.2 and 4.1.

From the contour plots in Figure 4.1, one can see that the dose rate decreased as the distance from the neutron source increased. This was true for all cases of neutron (left) and photon (right) dose rate distribution. This observation was expected because the dose rate should have decreased as the distance from the source term increased. Moreover, in all cases, the generator shielding and walls of the room played an important role in the reduction of the dose rates.

Also evident in Figures 4.1(a) and (c) is that the neutron dose rate was relatively higher outside the east wall (in the $-x$ direction) of the facility. The relative "spread" of neutron dose rates after the east wall, as compared to other directions, is clearly distinguishable in these figures. This is because the east wall was made of (lead-lined) brick; however, the west wall was made of 43.18 cm (17 in.) brick wall which provided an effective shielding for shielding the neutrons (see Figures 3.2(a), 4.1(a) and (c)). Materials with higher atomic numbers, like lead, were not a viable option for reducing neutron dose rates [11]. However, the vital role played by lead-lining in reducing photon dose rates is

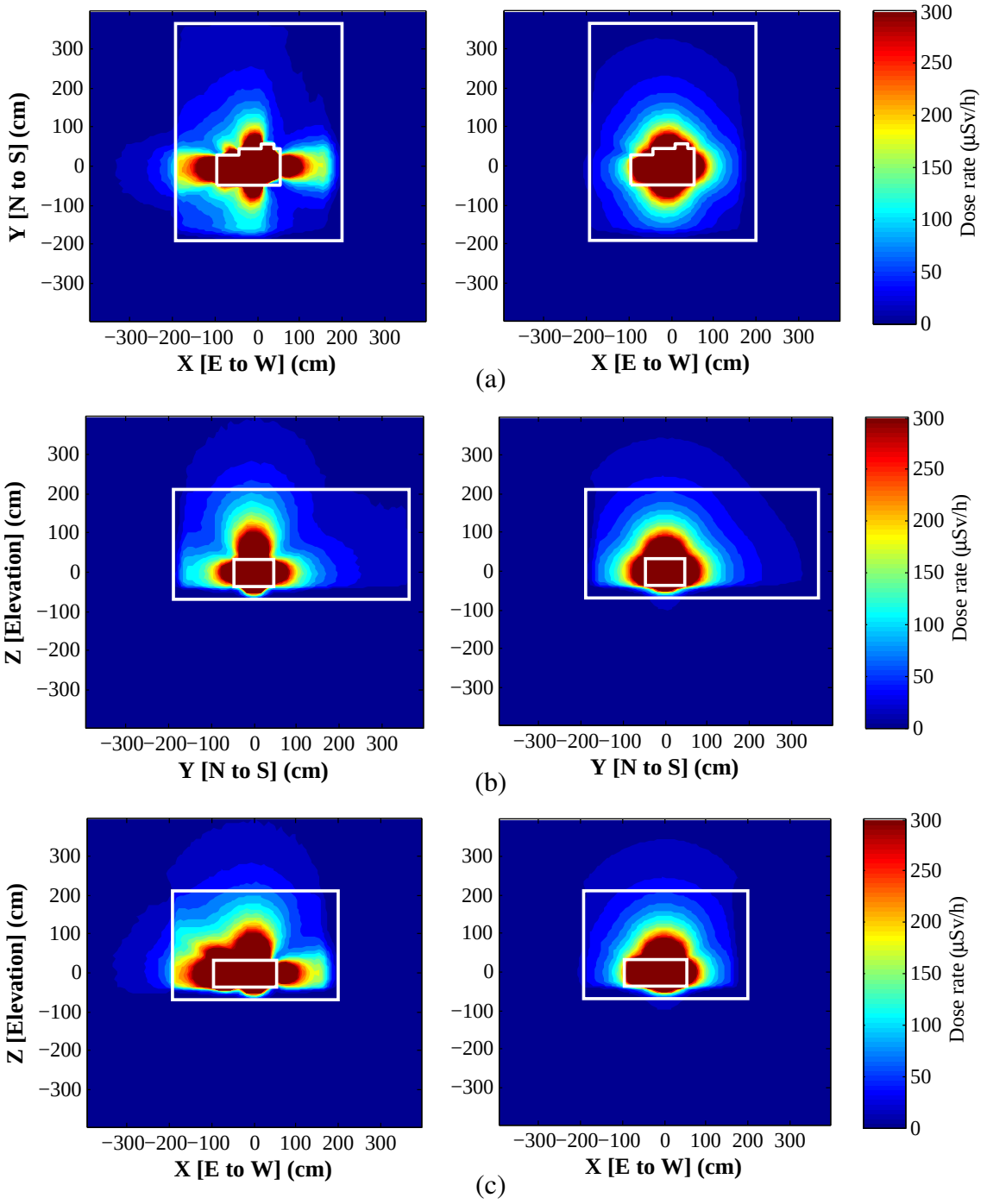

Figure 4.1 Neutron (left) and photon (right) dose rate contour plots (μSv/h), corresponding to central planes shown in Figure 3.2. (a) *xy* plane, (b) *yz* plane, (c) *xz* plane. Z represents the elevation difference from the source at origin. Outer boundaries of generator shielding and room walls are also shown for comparison.

clearly seen when one compares only the photon dose rates in the vicinity of the east wall (see Figures 4.1(a) and (c)).

The dose rates outside the south wall ($+y$ direction, see Figures 4.1(a)-(b)) were relatively less, even though the south wall had the same composition as the east wall. This was because the south wall was located at roughly twice the distance of the east wall from the neutron source, indicating that dose rates should be less at longer distances from the source term. Table 4.1 gives the maximum total dose rates outside each wall of the facility. It is also evident from Table 4.1 that the maximum total dose rate outside the south wall was less than the maximum value of the dose rate in the east direction.

As expected, the neutron and photon dose rates were relatively higher and more distributed above the roof of the generator room (in $+z$ direction, see Figures 4.1(b) and (c)). This was primarily because, for the MCNP model, it was assumed that the roof of the room was made of 2.54 cm (1 in.) thick wood. As already stated in section 2, this was a conservative estimate because, in a real situation, the room had a composite single material after the wood roof. Therefore, the neutron and photon dose rates were relatively higher in the regions above the facility.

Examining the neutron and photon dose contour plots in Figures 4.1(b)-(c), it is clear that the (lead-lined) concrete floor adequately served its purpose by reducing the neutron dose rates to the first floor of the building. However, a slight "bulge" in photon dose rates, just below the concrete floor (in $-z$ direction), can be seen in these plots. From Table]4.1 can be seen that the dose rate (in $-z$ direction) contributed by photons was approximately twice that of the dose rate contributed by the neutrons. This was primarily because the concrete was ideally suited for reducing the neutron dose rates. In our case, the neutron source lay at an elevation of about 36 cm from the floor. Therefore, it is expected that the photon dose rates to the first floor would be reduced if the height of the generator above the floor is increased, or additional lead will be inserted between the neutron generator and the floor.

Figure 4.2 gives an insight into the statistical uncertainties reported by the MCNP5 radiation transport code for the simulated neutron and photon dose rates for the three central planes. The statistical uncertainties in the neutron and photon dose rates, inside the shielding of the neutron generator, were less than 2.1% and 0.2%, respectively. Statistical uncertainties inside the generator room were less than 4.3% and 0.8% for neutron and photon dose rates, respectively. MCNP5 user's manual [18] specifies that the results provided by a tally with uncertainties of less than 10% can be considered as "generally reliable." It can be seen in Figures 4.2(b)-(c) that the statistical uncertainties were relatively higher for some directions. This can be explained by the fact that fewer neutrons were transmitted in those directions.

To provide an insight of the effectiveness of different materials in reducing the total dose rate, a plot of variation of dose rates at different distances was obtained. The variation in the total dose rate (along the central line) in $-x$ direction from the source towards the east wall (see Figures 3.1(a), 3.2(a) and (c)) is shown in Figure 4.3 . A combination of HDPE surrounded with lead, just in the immediate vicinity of the generator head, reduced the total dose rate by a factor of 16. This represented the importance of a combination of hydrogenated and higher atomic number materials in reducing the dose exposures. Thereafter, an HDPE block and 5% BPE reduced the total dose rate by a factor of about 4. The lead-lined brick wall also considerably reduced the dose rate by an approximate factor of 2.

To determine the maximum annual operating hours of the generator to keep the total dose rate within prescribed limits, the maximum total dose rates just outside the facility (walls, floor, and the roof) were utilized. These maximum total dose rates in the vicinity of the facility, as provided in Table 2.1, were used to predict the limited number of hours for operation of the generator annually. The limits imposed by the Nuclear Regulatory Commission on the dose received by individual members of the public (5 mSv) and an occupational annual exposure limit of 50 mSv were used to achieve this objective. As a

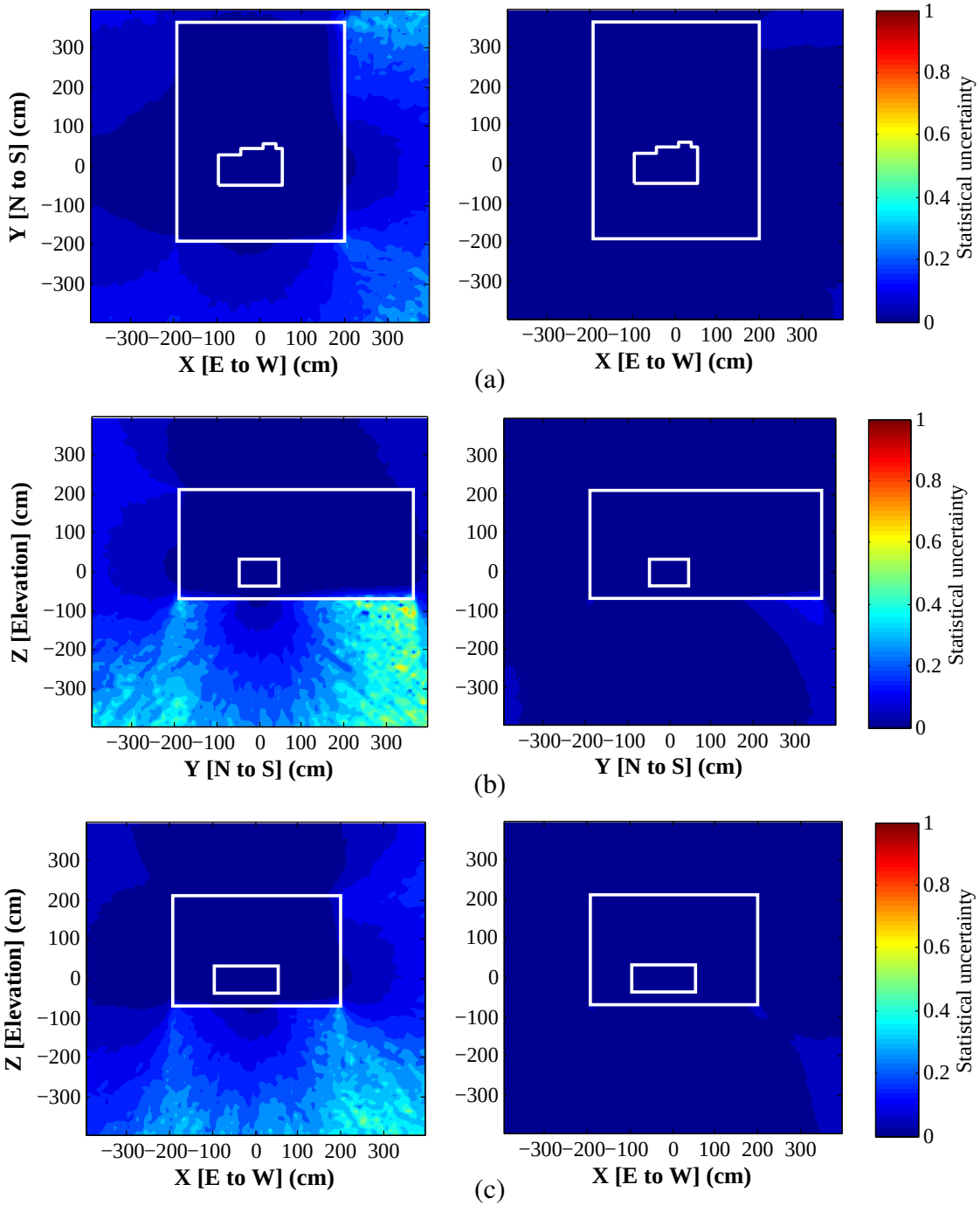

Figure 4.2 Statistical uncertainty associated with the neutron (left) and photon (right) dose rates, corresponding to central planes shown in Figure 3.2. (a) *xy* plane, (b) *yz* plane, (c) *xz* plane. Z represents the elevation difference from the source at origin. Outer boundaries of generator shielding and room walls are also shown for comparison.

conservative estimate, the maximum dose rate of 134.8 μSv/h at the east wall (see Table 4.1) was used to determine the annual limit of operating hours of the generator. Therefore, the maximum allowable operating hours of the generator, to keep the doses within the prescribed limits, were approximately 37.1 hours for the public and 371 hours for operators.

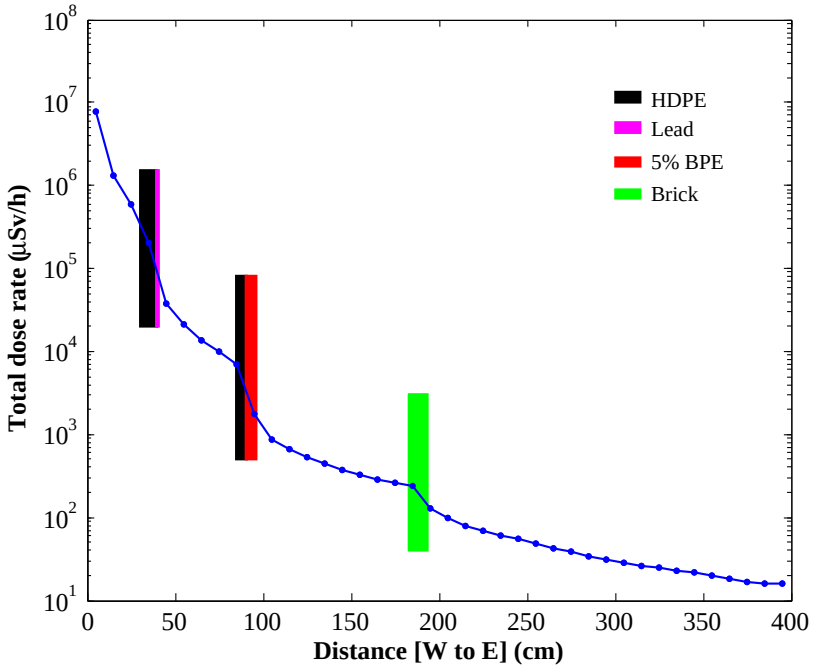

Figure 4.3 Variation in total dose rate from the source at origin toward the east wall of the neutron generator room. The effectiveness of different materials in reducing the dose rates can be observed.

It is worth noting that the room on the other side of the east wall (room 217 in Figure 1.2) is the room where the operation of the neutron generator will be controlled through a computer system. Therefore, it is possible to make this room a controlled area with access allowed for the authorized persons only. In this case, the annual limit of operating hours for the operator will be 371 hours (corresponding to a total dose rate of 134.8 μSv/h for occupational exposure limit of 50 mSv). However, the area is not currently isolated from public and, therefore, it is reasonable to say that existing shielding is enough to keep exposure to

Table 4.1 Maximum total dose rate for the vicinity of the facility (room 217A) where the neutron generator is installed. Neutron and photon dose rate contributions are also given.

Location	**Direction**	**Maximum total**	**Dose rate (μSv/h)**		**Uncertainty (%)**	
		dose rate (μSv/h)	**Neutron**	**Photon**	**Neutron**	**Photon**
East wall	$-x$	134.8	113.1	1.5	1.5	0.5
West wall	$+x$	16.6	12.9	4.1	4.1	1.2
North wall	$-y$	23.1	13.6	3.9	3.9	0.8
South wall	$+y$	21.9	13.5	4.0	4.0	0.8
Roof	$+z$	112.2	64.7	1.9	1.9	0.3
Floor	$-z$	47.5	16.1	3.6	3.6	0.4

the public within limits if the generator is operated for less than about 37.1 hours each year (corresponding to a total dose rate of 134.8 μSv/h for a 5 mSv exposure limit for individual members of public). If the operation of the generator beyond that time is desired, incorporation of more shielding in the east direction is suggested to minimize doses to the public working in the east side of the facility. Since about 84% of the maximum total dose rate in the east direction is contributed by neutrons, inclusion of additional hydrogenated and borated materials (like HDPE and BPE) in this direction is highly recommended (see Table 4.1). If required, movable or modular concrete blocks (as used and discussed in literature [10, 12, 13]) may serve as a suitable option for reducing the neutron dose rate in the east direction.

To determine the effectiveness of lead-lining of different walls and the floor in reducing the neutron and photon dose rates, an additional MCNP simulation was performed. As discussed in the previous section, everything else in the MCNP model was kept unchanged. The dose rates, without the lead-lining, were determined just in the vicinity of the respective (lead-lined) walls and the floor. It is important to note that these dose rates were determined at the same locations used to obtain the maximum total dose rate given in Table 4.1. The estimated neutron and photon dose rates, with and without the lead-lining, are given and compared in Table 4.2.

Table 4.2 Neutron and photon dose rates (μSv/h) with and without the lead-lining.

Location	**Direction**	**Neutron dose rate (μSv/h)**		**Photon dose rate (μSv/h)**	
		With lead	**Without lead**	**With lead**	**Without lead**
East wall	$-x$	113.1	114.9	21.7	25.4
South wall	$+y$	13.5	13.6	8.4	9.9
Floor	$-z$	16.1	17.3	31.4	41.4

The presence of lead reduced the neutron dose rates in the range of 0.9%–7.4%. As might be expected, the lead-lining does not play a significant role in reducing the dose rate contribution from neutrons. However, the reduction in photon dose rates, due to the lead-lining, is relatively more significant. The lead-lining reduces the photon dose rates in the range of 14.5%–24.1%. Therefore, the selection of shielding material is primarily dependent on the type of radiation to be shielded. The materials with higher atomic numbers are often a viable option for reducing the dose rate contribution from photons. However, these materials are relatively ineffective in shielding the neutrons [11]. The statistical uncertainties in the neutron and photon dose rates given in Table 4.2 lies in the range of 1.5%–4.0% and 0.4%–0.8%, respectively.

It is clear from Table 4.2 that the total dose rate is maximum in the east ($-x$) direction. Therefore, to observe the impact of lead-lining on annual limit of operating hours of the generator, the dose rates (with and without the lead-lining) were compared at the location in the vicinity of the east wall. The absence of lead-lining increased the total dose rate from 134.8 μSv/h to 140.2 μSv/h. In this (east) direction, the decrease in the contribution of photon dose rate, due to the lead-lining, is relatively more considerable ($\sim$14.5%) than the decrease in neutron dose rate ($\sim$1.6%). Moreover, the total dose rate is not significantly reduced (from 134.8 μSv/h to 140.2 μSv/h). This is because about 82% of the total dose rate is contributed by neutrons in this direction. Therefore, in the absence of lead-lining (with a total dose rate of 140.2 μSv/h), the annual operating hours of the neutron generator for public is approximately 35.7 hours (corresponding to a 5 mSv exposure limit for

individual members of public). In other words, the limit on annual hours of operation of the generator improves by approximately 3.9% (from 35.7 hours to 37.1 hours) with the introduction of lead-lining on the east wall. Although, the presence of lead-lining does not play a momentous role in improving the annual operating hours, its presence is important in reducing the doses, in accordance with the goal of maintaining doses as low as reasonably achievable (ALARA). The lead-lining, therefore, plays a reasonable role in achieving this objective and in improvement of the annual operating limit of the neutron generator.

5. CONCLUSIONS

In this article, the current shielding of the DD-109 generator installed in the Nuclear Engineering Department of Missouri S&T was modeled using the MCNP5 radiation transport simulation. The geometric and composition details of the generator room were also incorporated in the model to better approximate the dose rates outside the facility. The objective was to determine the exposure to the public and the operator if the generator is to be operated. The maximum total dose rates (contributed by neutrons and photons) in the vicinity of the facility (at each of the six sides) were also determined. These maximum total dose rates were utilized to make a conservative estimate of the annual limit of operational hours of the generator to correlate with the prescribed limits imposed by the Nuclear Regulatory Commission. It was shown that, if the generator is to be operated with the current shielding, the annual limit on operation of the generator would be approximately 37.1 hours (corresponding to a total dose rate of 134.8 μSv/h). Any operation of the generator for less than this time is, therefore, deemed to be safe as far as prescribed dose limits are concerned. If operation beyond this time is desired, it is suggested that more materials (suitable for shielding of neutrons) be employed on the east side of the generator room. An additional MCNP simulation was also performed to predict the effectiveness of lead-lining of east and south walls, and the floor. It was concluded that incorporation of lead-lining on the east wall improved the annual operating hours of generation by approximately 3.9%. To keep the dose rates to minimum, in accordance with the ALARA radiation safety principle, the lead-lining therefore plays a reasonable role in minimizing the total dose rate around the facility. In this study, the shielding effects of the titanium coated copper assembly that holds this target and the convective flowing cooling fluid system were not incorporated. The estimated dose rates and limit on annual hours of operation are, therefore, believed to be an overestimation to ensure safety from potential radiation exposure.

ACKNOWLEDGMENTS

The authors are thankful to Mr. Charles Gary, Adelphi Technology, for providing detailed information about the geometry of the DD-109 neutron generator.

REFERENCES

[1] D. L. Williams, J. H. Vainionpaa, G. Jones, M.A. Piestrup, C. K. Gary, J. L. Harris, M. J. Fuller, J. T. Cremer, B. A. Ludewigt, J. W. Kwan, J. Reijonen, K. N. Leung, and R. A. Gough. High intensity, pulsed, DD neutron generator. In *Applications of Accelerators in Research and Industry, Twentieth International Conference, Fort Worth, Texas*, pages 10–15, 2008.

[2] S. S. Nargolwalla and E. P. Przybylowicz. *Activation analysis with neutron generators*. Wiley and Sons, NewYork, 1973.

[3] IAEA Radiation Technology Reports No. 1. Neutron generators for analytical purposes. Technical report, 2012.

[4] J.T. Cremer, D.L. Williams, C.K. Gary, M.A. Piestrup, D.R. Faber, M.J. Fuller, J.H. Vainionpaa, M. Apodaca, R.H. Pantell, and J. Feinstein. Large area imaging of hydrogenous materials using fast neutrons from a DD fusion generator. *Nuclear Instruments and Methods in Physics Research A*, 675:51–55, 2012.

[5] M.K. Fuller, M.A. Piestrup, C.K. Gary, J.L. Harris, G. Jones, J.H. Vainionpaa, D.L. Williams, J.T. Cremer, A. Bell, G. McRae, et al. Long-lifetime high-yield neutron generators using the DD reaction. 2009.

[6] MCNP-A general Monte Carlo N-Particle transport code, version 5. Los Alamos National Laboratories, Los Alamos, New Mexico, 2011.

[7] J. Katalenich, M. Flaska, S. A. Pozzi, and M. R. Hartman. High-fidelity MCNP modeling of a D-T neutron generator for active interrogation of special nuclear material. *Nuclear Instruments and Methods in Physics Research Section A*, 652(1):120–123, 2011.

[8] J.C. Liu and T.T. Ng. Monte Carlo calculations using MCNP 4B for an optimal shieding design for a 14 MeV neutron source. *Radiation Protection Dosimetry*, 83 (3):257–62, 1999.

[9] D.L. Chichester and G.D. Pierce. Analysis of a shield design for a DT neutron generator test facility. *Applied Radiation and Isotopes*, 65(10):1125–1133, 2007.

[10] D.L. Chichester, E.H. Seabury, J.M. Zabriskie, J. Wharton, and A.J. Caffrey. Dose profile modeling of Idaho National Laboratory's active neutron interrogation laboratory. *Applied Radiation and Isotopes*, 67(6):1013–1022, 2009.

[11] D.L. Chichester and B.W. Blackburn. Radiation fields from neutron generators shielded with different materials. *Nuclear Instruments and Methods in Physics Research Section B*, 261(1):845–849, 2007.

[12] J. E. Turner. *Atoms, radiation, and radiation protection*. John Wiley & Sons, 2008.

[13] NCRP Report No. 144. Radiation protection for particle accelerator facilities. Technical report, National Council on Radiation Protection and Measurements, Bethesda, MD, 2005.

[14] Y. Elmahroug, B. Tellili, and C. Souga. Calculation of fast neutron removal cross-sections for different shielding materials. *International Journal of Physics and Research (IJPR)*, 3(2):7–16, 2013.

[15] R.J. McConn Jr., J.C. Gesh, R.T. Pagh, R.A. Rucker, and R.G. Williams III. Compendium of material composition data for radiation transport modeling. *PNNL-15870 Rev*, 1(4), 2011. URL `http://www.pnnl.gov/main/publications/external/technical_reports/PNNL-15870Rev1.pdf`.

[16] D.J. Whalen, D.A. Cardon, J.L. Uhle, and J.S. Hendricks. MCNP: Neutron benchmark problems. Technical report, Los Alamos National Lab., NM (United States). Funding organisation: USDOE, Washington, DC (United States), 1991. URL `http://www.iaea.org/inis/collection/NCLCollectionStore/_Public/23/033/23033166.pdf`.

[17] N. Petoussi-Henss, W.E. Bolch, K.F. Eckerman, A. Endo, N. Hertel, J. Hunt, M. Pelliccioni, H. Schlattl, M. Zankl, et al. Conversion coefficients for radiological protection quantities for external radiation exposures. *Annals of the ICRP*, 40(2), 2010.

[18] X-5 Monte Carlo Team. MCNP-A general Monte Carlo N-Particle transport code, version 5. 2003.

III. ADJOINT ACCELERATION OF MONTE CARLO SIMULATIONS USING SCALE: A RADIATION SHIELDING EVALUATION OF THE NEUTRON GENERATOR ROOM AT MISSOURI S&T

Manish K. Sharma, Ayodeji B. Alajo, Xin Liu

Missouri University of Science & Technology,

Nuclear Engineering, Rolla, MO, USA

ABSTRACT[§]

A deuterium-deuterium accelerator-type neutron generator was installed in the Nuclear Engineering Department at Missouri University of Science and Technology (Missouri S&T). This generator is shielded by different hydrogenated and non-hydrogenated materials to reduce the dose rates in the vicinity of the facility. In the work presented in this paper, both SCALE6 and MCNP5 radiation transport codes were used to conduct two independent simulations. The new shielding analysis tool of SCALE6—MAVRIC, with the automatic variance reduction technique of SCALE6, was utilized to estimate and compare the dose rates from the unbiased MCNP simulation. The ultimate goal of this study was to compare the computational effectiveness offered by employing the MAVRIC sequence in the modeling of the neutron generator facility at Missouri S&T.

Keywords: Neutron generator shielding, D-D neutron generator, Monte Carlo, Variance, Dose

[§]Published in Nuclear Instruments and Methods in Physics Research Section A (2015).

1. INTRODUCTION

Monte Carlo simulations are considered the most accurate method for solving dose rates in a radiation field. However, the computation time required for many practical problems involving deep-penetration is prohibitive. Over the past several decades, various techniques have been developed to reduce the variance in dose rates and accelerate the Monte Carlo simulations [1–10]. Among these developments, the hybrid Monte Carlo/Deterministic methods are the favored techniques for radiation shielding problems [8–10]. The Oak Ridge National Laboratory recently developed a new shielding analysis tool in the SCALE6 code system [11]. This new tool, known as MAVRIC (Monaco with Automated Variance Reduction using Importance Calculations), employs a hybrid deterministic-stochastic method to automatically generate variance reduction parameters for Monte Carlo simulations. MAVRIC is based on the Consistent Adjoint Driven Importance Sampling (CADIS) and Forward CADIS (FW-CADIS) methodologies, which use the concept of an importance map and biased source distribution to accelerate Monte Carlo simulations (a more detailed description can be found in [8–11]). In the past, it has been shown that this hybrid technique serves as an appropriate method for the shielding analysis of nuclear reactors [12–15].

In this work, this new shielding analysis tool (MAVRIC), with the automatic variance reduction technique of SCALE6 radiation transport code, was utilized to estimate the dose rates in and around the neutron generator facility at Missouri University of Science and Technology (Missouri S&T).

A deuterium-deuterium (D-D) accelerator-type neutron generator (model: DD-109, manufactured by Adelphi Technology) was recently installed in the Nuclear Engineering Department at Missouri S&T. The operation of this generator will produce fast neutrons of approximate energy 2.5 MeV through D-D fusion reactions ($^{2}H + {}^{2}H \rightarrow {}^{3}He + n$). The detailed working mechanism and the applications of neutron generators that produce fast

neutrons through deuterium-deuterium and deuterium-tritium fusion reactions have been discussed extensively in the literature [16–20]. The operation of the generator at Missouri S&T will increase radiation exposure around the facility. Therefore, to reduce the dose rates in and around the facility, due to the neutrons and secondary photons, the generator has been shielded with different materials. Shielding of neutrons is a challenging problem because of the fact that dose contributions from both the neutrons and the photons should be considered. Therefore, the generator was shielded with different materials (e.g., high-density polyethylene, lead, and 5 wt.% borated polyethylene). Moreover, some walls of the generator room were also lead-lined to further reduce the dose rates around the facility.

A Monte Carlo N-Particle (MCNP) radiation transport code [21, 22] was recently used to develop a model of the neutron generator and its facility. An MCNP simulation was then performed to estimate the generator's annual hours of operation in order to keep the dose rates within the prescribed limits. This problem is a typical example of a deep-penetration shielding problem where the attenuation of the beam is considerably higher. Thus, it was difficult to obtain good statistics (i.e., low relative uncertainty) in the regions of interest without sacrificing computation time. Therefore, in the work presented in this paper, attempts were made to speed up the simulations by utilizing the automated variance reduction technique of the MAVRIC tool. The ultimate goal was to compare the dose rates and statistical uncertainties from a SCALE simulation with those from a Monte Carlo simulation and thereby evaluate the relative computation efficiency of the SCALE simulation. The concept of Figure-of-Merit was utilized to determine the relative computation efficiency and speedup of the SCALE simulation.

2. FACILITY LAYOUT AND ANALYTICAL CALCULATIONS

The physical placement of the DD-109 accelerator-type neutron generator at Missouri S&T is illustrated in Figure 2.1. The generator, which is installed in room 217A on the second floor of the Fulton Hall building, will be operated from an adjacent room (no. 217), as shown in Figure 2.1. For spatial clarity, a zoomed image of room 217A is also shown. As already discussed in the previous section, this type of generator utilizes D-D fusion reactions to produce fast neutrons with an approximate energy of 2.5 MeV. The V-shaped copper target (where the D+ ions strike) is approximately 1.02 cm thick and has a titanium coating that is approximately 0.102 mm thick. The initial bombardment of D+ ions results in the formation of titanium hydride on the target's surface. The subsequent bombardment of D+ ions at the target initiates the D-D fusion reactions that produce fast neutrons. For a sufficient reduction of dose rates (due to generated neutrons and secondary photons) in and around the facility, it is imperative that sufficient shielding be provided around the generator and the facility. Various materials (e.g., high-density polyethylene, borated polyethylene, and lead) have been used to achieve this objective. The V-shaped target and the current shielding of the generator are depicted in Figure 2.2(b). The generator was first surrounded by high-density polyethylene (HDPE) to efficiently thermalize the fast neutrons. Hydrogenated materials (such as HDPE) are always a preferred option for this purpose. The (n,γ) capture reactions in the HDPE also results in dose rate contribution from photons. Due to its high atomic number, lead is the preferred choice for attenuating photons. Therefore, the HDPE has been surrounded by a 0.64 cm (0.25 in.) thick lead box to reduce the dose rate contribution from photons (see Figure 2.3).

This entire configuration has been surrounded by 5.08 cm (2 in.) thick 5 wt.% borated polyethylene (BPE) to absorb the thermalized neutrons. The shielding's shape was chosen to effectively cover the generator by utilizing rectangular pieces of polyethylene.

Figure 2.1 Layout of second floor of the Fulton building where the generator is located. Also shown is a zoomed image of the room (217A) where the generator is installed.

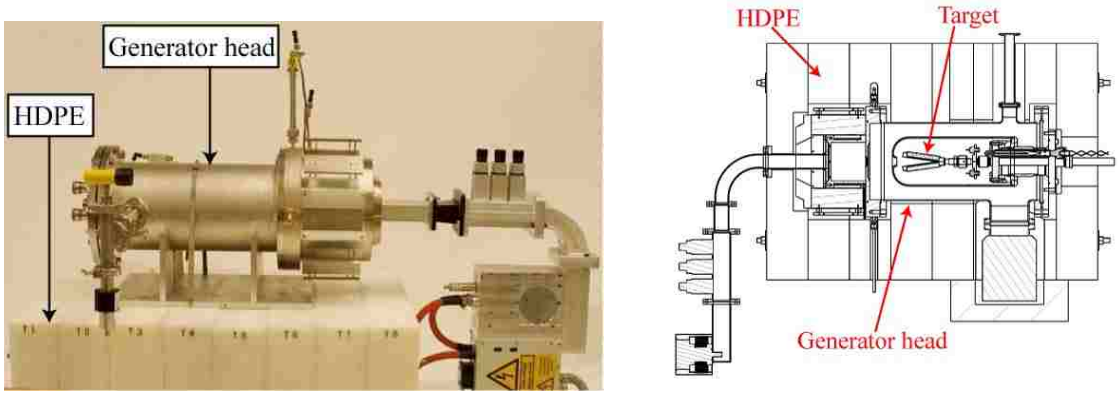

(a) (b)

Figure 2.2 (a) DD-109 neutron generator head and HDPE blocks used for shielding of generator. (b) Cutaway of a neutron generator and the surrounding HDPE blocks. The V-shaped target, where the neutrons are produced, is also shown (Image courtesy of Adelphi Technology, Inc.).

This design also offers the advantage of obtaining a more “open” space where the samples can be placed and irradiated (see Figure 2.3(b)).

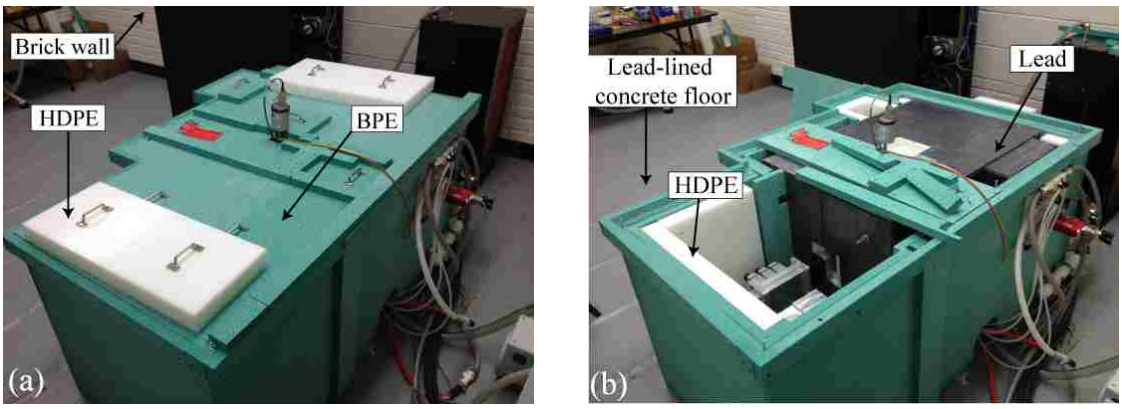

Figure 2.3 (a) DD-109 generator shielding. (b) Different materials used in the shielding. (The top BPE cover is removed for a better perspective.) The place where samples will be irradiated is also shown.

It is worth noting that the walls, roof, and floor of the generator room also provide shielding to the neutrons and secondary photons. The composition and the thickness of each wall are listed in Table 2.1.

Some of the walls of the generator room have also been lead-lined to reduce the dose contribution from the photons. The eastern and southern walls each have a lining of 0.32 cm thick lead to reduce the dose rates in the adjoining rooms (rooms 217 and 218 in Figure 2.1). Since the generator is elevated approximately 36 cm from the floor, the concrete floor has also been lined with 0.64 cm thick lead to reduce the exposure (due to secondary photons) to the persons working on the building's first floor. The effectiveness of lead-lining in reducing the neutron and photon dose rates is discussed in [21]. The room's roof in the developed SCALE model was assumed to be made of a 2.54 cm (1 in.) thick wood covering only. In reality, the roof is made of a composite material located above the wood. This assumption was made so that the simulated dose rates were an overestimation of the actual values. Moreover, the MCNP simulation that was recently performed[21] was also based on the same assumption. Therefore, maintaining the same assumptions for both models was crucial for a justified comparison between these dose rates (obtained from the MCNP) and those obtained from the SCALE.

Table 2.1 Composition and dimensions of different walls of the generator room.

Location	Composition	Thickness (cm)
East wall	Brick	10.16
West wall	Brick	43.18
North wall	Brick	32.39
South wall	Brick	10.16
Roof	Wood	2.54
Floor	Concrete	32.39

2.1. ANALYTICAL CALCULATIONS

An analytical estimate of the neutron dose rate was made at the reference point. The objective was to see how close the neutron dose rate from SCALE simulation was to this estimate. The NCRP Report No. 144 recommends the "removal cross-section" method for the estimation of dose rate from neutrons of energy less than 30 MeV [23] shielded with hydrogenous materials. This approach, however, requires information of the buildup factor—which accounts for the dose contribution from scattered neutrons. Therefore, an alternative approach (given in [17]) was used to theoretically estimate the dose rate. The neutron dose rate at a reference position 1 m away from the neutron source in the east direction (position A in Figure 2.4) is given by

$$DE_t = DE_0 * C * e^{-t/\lambda} \tag{1}$$

where DE_t and DE_0 are the dose equivalent values at a particular position with and without a shield of thickness t, λ is the relaxation length, and C is a constant that incorporates the scattering factor for the correction. The neutrons, when traveling to reference position A, will encounter approximately 14.3 cm of HDPE and approximately 5.08 cm of BPE. Since lead is practically ineffective in attenuating the neutrons [21, 24], the attenuation from the 0.64 cm lead encountered in this direction was ignored. Furthermore, the HDPE, BPE, and

paraffin had very similar densities and neutron removal cross-sections [25, 26]. Therefore, the relaxation length of paraffin provided in [17] was used in the calculation using Eq. ((1)).

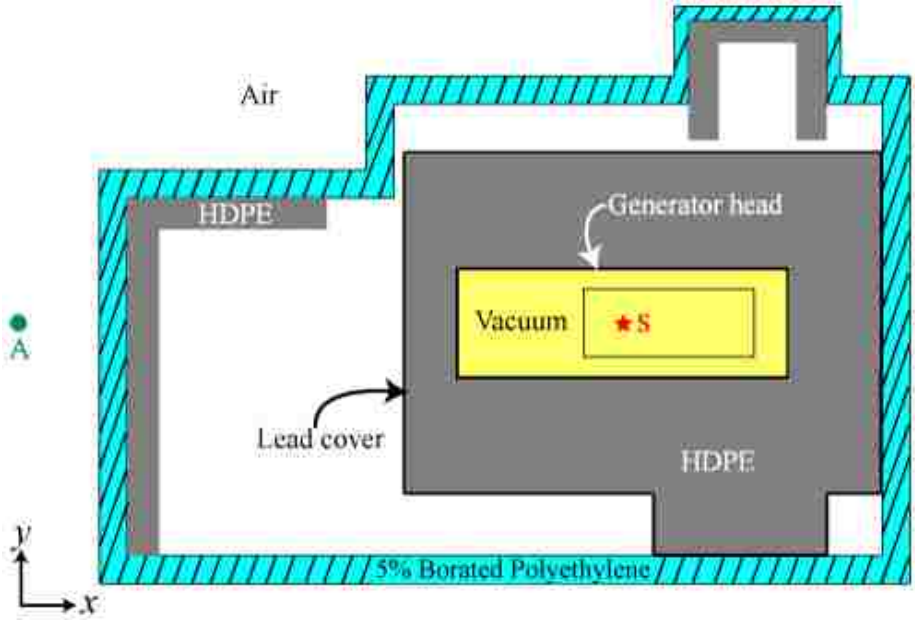

Figure 2.4 Cutaway diagram of the generator's shielding (central plane, *xy* view). The neutron source (indicated by a red star) is assumed to be a point source at the origin. Also shown is the reference position (A) where the analytical calculation was performed. (For interpretation of the references to color in this figure legend, the reader is referred to the web version of this article.)

The unshielded dose rate (DE_0) at a distance of R cm away from a neutron source of strength S neutrons per second is given by

$$DE_0 = \frac{Sq}{4\pi R^2} \tag{2}$$

where q is the dose-equivalent rate per unit neutron fluence rate (in Sv h^{-1} per neutron cm^{-2} s^{-1}, provided in [26]). For a neutron source emitting 2.5 MeV neutrons with a rate of 2×10^9 neutrons/s, the unshielded and shielded neutron dose rates (at reference

position A) were calculated to be 22.25 mSv/h and 0.99 mSv/h, respectively. Thus, the generator's shielding reduced the neutron dose rate by an approximate factor of 22 (in the east direction). This observation highlights the importance of incorporating hydrogenated shielding materials for effective reduction of neutron dose rates. The analytical estimate at the reference position (with shielding) was also found to be reasonably close to the dose rate value obtained for that position from the SCALE simulation: 1.06 mSv/h, with a relative uncertainty of approximately 0.8%. Details of the developed SCALE model and the simulation performed are given in the following section.

3. SCALE MODELING AND METHODOLOGY

The details of composition and dimensions of the generator head, shielding, and the facility were used to develop a SCALE model. To simplify the analysis, a point neutron source of energy 2.5 MeV and strength of 2×10^9 neutrons/s was assumed to be at the origin. This assumption was a conservative estimate because the attenuation from the V-shaped titanium-coated copper target was neither considered nor incorporated in the model. The neutron source (i.e., the target) was surrounded by an aluminum shroud approximately 0.15 cm (0.06 in.) thick and 12.7 cm (5 in.) in diameter. This shroud was further surrounded by a stainless steel outer wall that was approximately 0.28 cm (0.11 in.) thick with a 20.32 cm (8 in.) diameter. Adelphi Technology provided the generator head's dimensions and compositions. The generator head was assumed to be cylindrical in shape, which is a reasonable assumption with regard to its original shape (see Figure 2.2). The compendium of material composition data [27] was used to obtain details on the composition of different materials, information that is necessary for SCALE modeling. The composition and density information of the different materials used to model the generator head, its shielding, and the facility are listed in Table 3.1. Details of the generator head, the target, and the cooling mechanism are discussed in [21]. A final SCALE model of the generator head, shielding, and facility was then developed. The 3D views of this model, obtained using the KENO3D visualization tool [28], are illustrated in Figure 3.1.

Table 3.1 Composition of different materials used in MCNP modeling of the generator head, its shielding, and the facility [27, 29].

Element	**Material (weight fraction)**								
	HDPE	**BPE**	**Lead**	**Brick (common silica)**	**Concrete (regular)**	**Wood**	**Air**	**Stainless Steel (304)**	**Aluminum (alloy 6061-O)**
Al				0.005	0.034				0.972
Ar							0.0128		
B		0.0469							
C	0.8563	0.7232				0.497	0.0001	0.0004	
Ca				0.014	0.044	0.002			
Cr								0.19	0.002
Cu									0.0028
Fe				0.007	0.014			0.7017	0.0041
H	0.1437	0.127			0.01	0.0596			
K						0.002			
Mg						0.002			0.01
Mn								0.01	0.0009
N						0.005	0.7553		
Na					0.029				
Ni								0.0925	
O		0.1029		0.525	0.532	0.4274	0.2318		
P								0.0002	
Pb			1						
S						0.005		0.0002	
Si				0.449	0.337			0.005	0.006
Ti									0.0009
Zn									0.0015
Density (g/cm^3)	0.93	0.937	11.35	1.8	2.3	0.64	0.0012	8	2.7

After the geometric SCALE model was developed, it was important to establish the tally and the automatic variance reduction parameters. Since the total dose rate is contributed by both the neutrons and the (secondary) photons, respective neutron and photon mesh tallies to cover the entire facility (approximately 500 cm $\times$ 600 cm $\times$ 350 cm in dimension) were created. The FW-CADIS methodology was then adopted to optimize the Monte Carlo simulations so that various tallies have more uniform relative uncertainties. The FW-CADIS approach first performed a quick discrete ordinates calculation, using the S_N method, to estimate the expected tally results. The S_N method is a deterministic methodology for numerically solving the Boltzmann transport equation and its related adjoint equation [30]. Then, an adjoint S_N calculation was performed to construct the adjoint source. Thereafter, the adjoint source, corresponding to each tally, was weighted inversely by those forward tally estimates obtained in the first S_N calculation. Finally, the weighted adjoint flux was used to create the importance map.

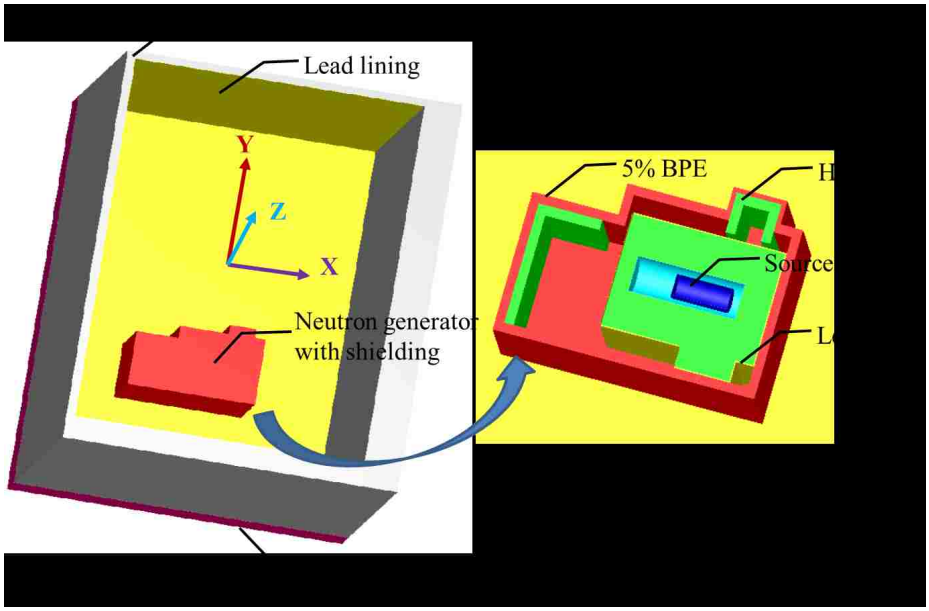

Figure 3.1 3D views of the generator facility and its shielding. (The facility's roof is not shown.)

The mesh tallies for neutron and photon dose rates were constructed uniformly along three central planes passing through the neutron source: *xy*, *yz*, and *xz*. A total of 111,996 (51 $\times$ 61 $\times$ 36) bins were created, with each bin of size 10 cm $\times$ 10 cm $\times$ 10 cm. To perform a deterministic S_N calculation, a grid geometry overlaying the physical geometry was created. This grid mesh size was made relatively large to improve the computational efficiency. Therefore, a grid mesh of 41 $\times$ 53 $\times$ 30 cells was created. Since the grid mesh size was not uniform, additional grid cells were constructed in the peripherals of the facility. The S_N calculations used the default S_8 quadrature and P_3 Legendre order. These calculations used 27 neutron energy groups and 19 photon energy groups. In the final dose rate calculations, however, 200 neutron energy groups and 47 photon energy groups were used. In both cases, the energy groups were taken from the ENDF/B-VII library. The simulated neutron and photon dose rate contour plots at three central planes, obtained from the SCALE simulation, are illustrated and discussed in the following section.

As already discussed, the recently developed MCNP model [21] was computationally expensive when obtaining reasonable uncertainties for the dose rates. The computation time of MCNP simulation for a particle history of 1×10^9 on different computer systems is given in Table 3.2.

Table 3.2 Computation time on different computer systems for a previously performed MCNP simulation [21].

Computer system configuration	**Computation time (days)**
Intel Core2Duo 2.2 GHz processor (2 GB RAM)	12.4
Intel Core2Quad 2.66 GHz processor (8 GB RAM)	9.5
Intel Xenon 3.33 GHz processor (48 GB RAM)	6.4

The computational expensiveness of this Monte Carlo simulation was, therefore, prohibitive. Thus, in this study an attempt was made to accelerate the Monte Carlo simulation by generating the variance reduction parameter using the MAVRIC sequence. To gain an insight into the computational effectiveness of the variance reduction technique, results from the SCALE simulation and an analogy (unbiased) MCNP simulation were compared. The concept of Figure-of-Merit (FOM) was utilized to achieve this objective. It was defined as

$$FOM = \frac{1}{RE^2 \times T} \tag{3}$$

where RE is the relative uncertainty in the dose rate and T is the total computation time taken for the simulation [31]. As indicated by its definition above, the value of FOM includes consideration of both the resultant relative error of the sample mean and the computer time necessary to achieve this relative error. A comparison of FOM values for two different and independent simulations (Monte Carlo and SCALE) is made in next section.

4. RESULTS AND DISCUSSION

The model discussed in the previous section was used to perform a SCALE simulation for a computation time of 800 minutes. The neutron dose rate contour plots (in Sv/h) for three central planes, obtained from the SCALE simulation, are shown in Figure 4.1. The statistical uncertainty corresponding to the dose rate at each position is depicted in Figure 4.2. Similarly, the photon dose rate contour plots (in Sv/h) and their respective statistical uncertainties are given in Figures 4.3 and 4.4, respectively. For a better understanding of the distribution of dose rates in and around the facility, the outer boundaries of the generator shielding and the facility are also shown.

The vital role played by the generator's shielding and the facility's walls in reducing the dose rates is shown in Figures 4.1 and 4.3. As expected, the neutron and photon dose rate decreased as the distance from the source increased. This finding is supported by the fact that the neutron and photon dose rate decreased approximately by the order of 10^8 and 10^5. The dose rates were relatively higher just outside the east wall, as observed in previously obtained results [21]. The effectiveness of a lead-lined concrete floor can also be seen in Figures 4.1(b) and 4.1(c). These dose contours also considerably matches to those obtained from a previous MCNP simulation.

The estimated dose rates had reasonably good statistics (i.e., low uncertainty) in regions located inside the facility (see Figures 4.2 and 4.4). Inside the shielding, the statistical uncertainties in the neutron and photon dose rates were less than 4.1% and 1%, respectively. These respective uncertainties were less than 6.8% and 4.6% inside the generator facility. The regions, that were primarily near the facility's walls, had relatively higher uncertainties. This observation was based on the fact that fewer particles were registered in those regions.

The primary focus of this work was to compare the computational effectiveness of employing a variance reduction technique in the modeling of a generator facility. Thus,

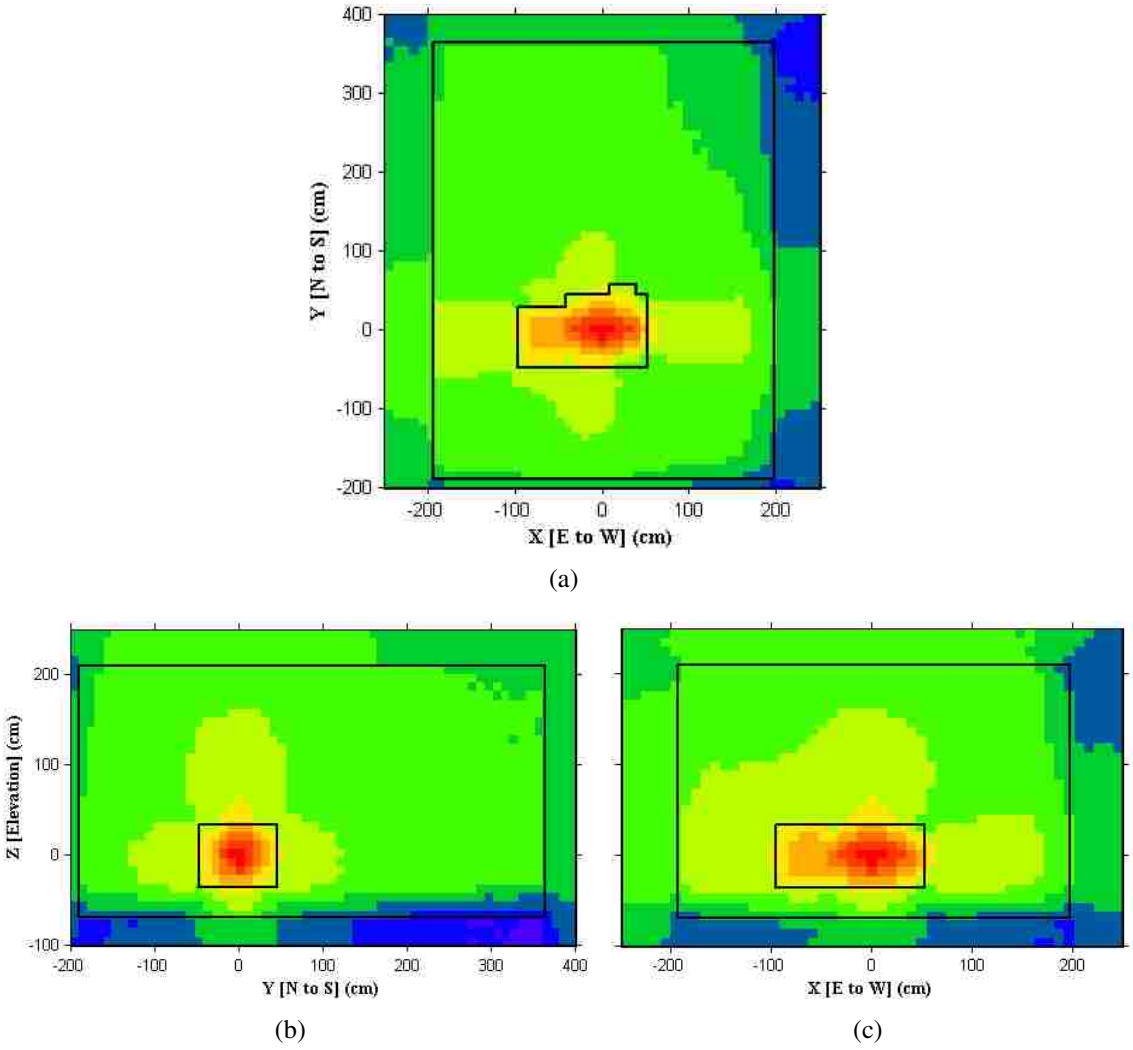

Figure 4.1 Neutron dose rate contour plots along the three central planes passing through the neutron source at origin. Outer boundaries of the generator's shielding and the facility's walls are also shown for comparison.

the computational efficiencies of two independent SCALE6 and MCNP5 simulations were compared to one another. For this purpose, we compared the Figure-of-Merit of dose rates at six positions near the facility (where the maximum total dose rates had been earlier reported [21]). The two simulations were performed on the same computer system, for the same computation time, to create a reliable comparison. The SCALE simulation was performed using the developed model and the automatic variance reduction technique of

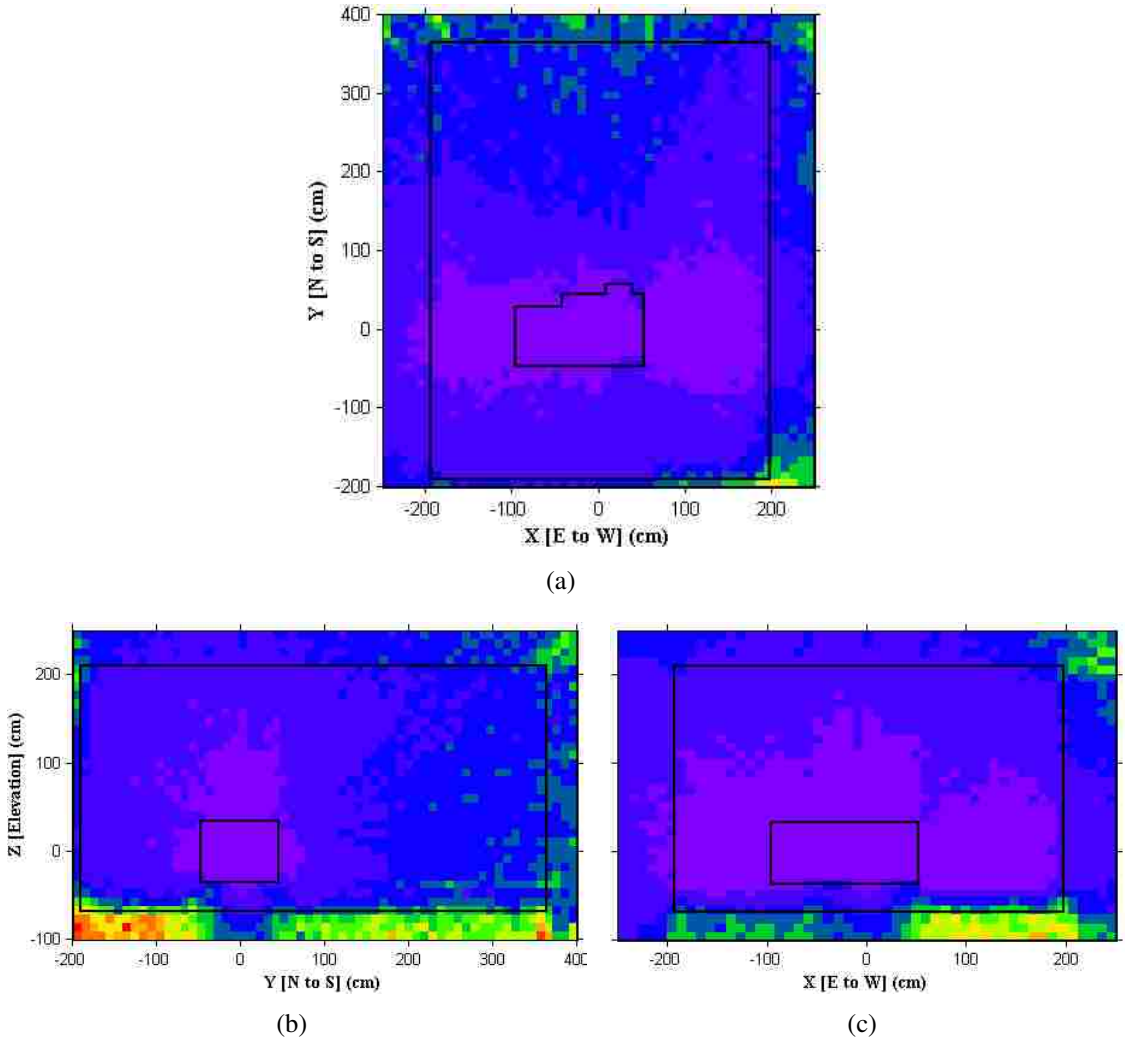

Figure 4.2 Contour plots showing the relative uncertainty in the neutron dose rate along the three central planes passing through the neutron source at origin.

the MAVRIC sequence, as already discussed in the previous section. The MCNP model developed previously was used for the Monte Carlo simulation [21].

Both of these simulations were performed for time duration of 800 minutes on a computer system with an Intel Xenon 3.33 GHz processor and a 48 GB RAM. The objective was to compare the neutron and photon dose rates at six positions near the facility where the total dose rates were maximum. These dose rates are given in Tables 4.1 and 4.2, respectively. The FOM values are also reported for each of the dose rates. The importance

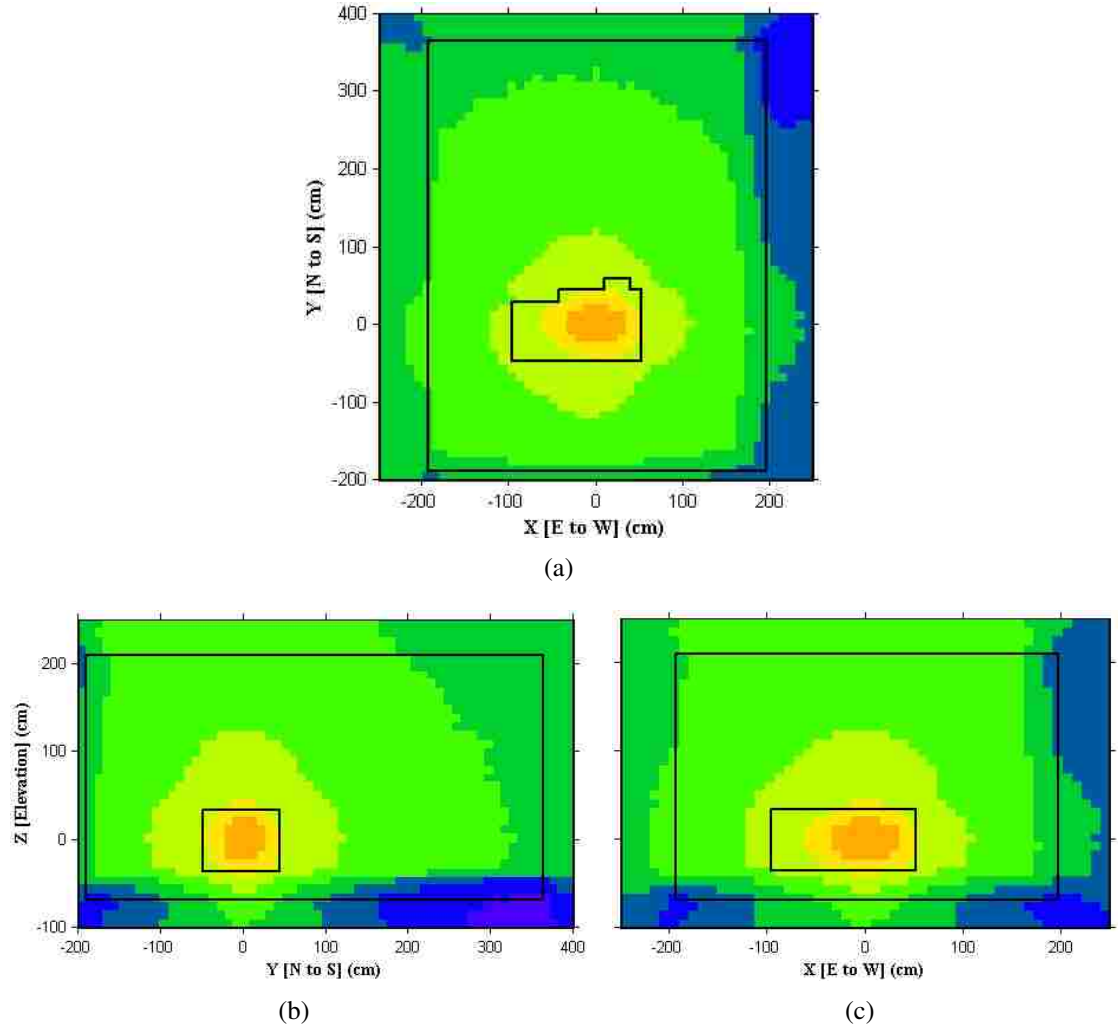

Figure 4.3 Photon dose rate contour plots along the three central planes passing through the neutron source at origin.

of utilizing the variance reduction technique to obtain dose rates with less uncertainty for the same computer time can be seen in Table 4.1. The speedup represents the ratio of FOM values from the SCALE and MCNP simulations. The average computational speedup of 11.3 demonstrates the momentous role played by variance reduction technique in improving the computational efficiency.

Improvement in the photon dose rate uncertainties from the SCALE simulation was not very significant, as evidenced in Table 4.2. It was even worse in most of the locations (see Table 4.2). This finding is justified because the goal of the FW-CADIS

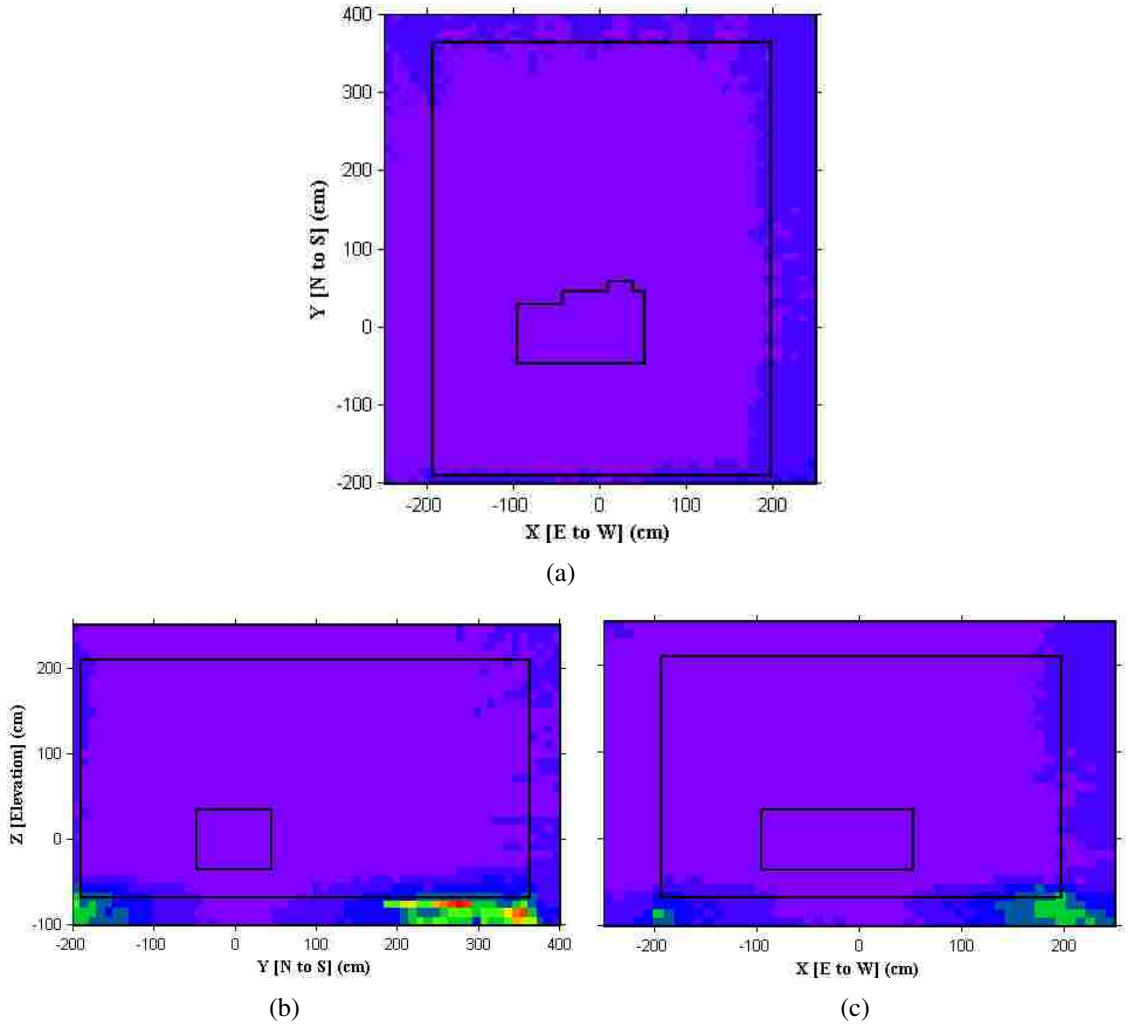

Figure 4.4 Contour plots showing the relative uncertainty in the photon dose rate along the three central planes passing through the neutron source at origin.

method is to converge neutron and photon dose tallies to similar relative uncertainties. The adjoint source (i.e., importance) corresponding to the neutron and photon dose tallies needs to be weighted inversely by the neutron and photon fluence value in the FW-CADIS approach. This leads to much reduced relative uncertainty for the neutron dose tally and slightly increased relative uncertainty for the photon dose tally. Additionally, the dose rate contribution from neutrons was approximately 85% of the total dose rate in the east direction. Therefore, the speedup in the neutron dose rate simulation was more important.

Table 4.1 The neutron dose rate contribution near the facility (where maximum total dose rates were earlier reported [21]). Dose rates from the SCALE and unbiased MCNP simulations were compared for $T = 800$ min.

Location	**Direction**	**Neutron dose rate (μSv/h)**		**Neutron relative uncertainty (%)**		**Neutron dose rate FOM (min^{-1})**		**Speedup**
		MCNP	**SCALE**	**MCNP**	**SCALE**	**MCNP**	**SCALE**	
East wall	$-x$	113.8	114.6	5.0	1.6	0.500	4.883	9.8
West wall	$+x$	12.9	13.8	14.1	2.5	0.063	2.0	31.7
North wall	$-y$	12.1	14.7	14.5	4.2	0.059	0.709	12.0
South wall	$+y$	13.4	13.1	13.6	6.9	0.068	0.263	3.9
Roof	$+z$	63.8	68.1	6.4	3.3	0.305	1.148	3.8
Floor	$-z$	17.4	18.1	11.8	4.6	0.090	0.591	6.6

Table 4.2 Photon dose rate contribution near the facility (where maximum total dose rates were earlier reported [21]). Dose rates from the SCALE and unbiased MCNP simulations were compared for $T = 800$ min.

Location	**Direction**	**Photon dose rate (μSv/h)**		**Photon relative uncertainty (%)**		**Photon dose rate FOM (min^{-1})**		**Speedup**
		MCNP	**SCALE**	**MCNP**	**SCALE**	**MCNP**	**SCALE**	
East wall	$-x$	20.4	23.4	1.7	2.1	4.325	2.834	0.7
West wall	$+x$	3.8	3.6	4.2	3.7	0.709	0.913	1.3
North wall	$-y$	9.3	10.6	2.6	3.2	1.849	1.221	0.7
South wall	$+y$	8.2	8.7	2.7	3.7	1.715	0.913	0.5
Roof	$+z$	46.5	44.4	1.2	2.4	8.681	2.17	0.2
Floor	$-z$	30.7	32.5	1.4	2.7	6.378	1.715	0.3

Better insight into the uncertainty distribution can be observed in the relative uncertainty histograms illustrated in Figure 4.5. Figures 4.5(a)-(b) show the fraction of voxels that has relative uncertainty that is less than a particular amount. Relative low and uniform uncertainties, throughout the entire mesh tally of neutron or photon dose rates, indicate that the FW-CADIS technique is better than the analog Monte Carlo simulation. The distribution of uncertainties is given for the two independent MCNP and SCALE simulations performed for a duration of 800 minutes. A histogram of uncertainties from the MCNP

simulation performed previously [21] for a particle history of 1×10^9 ($T = 6.4$ days) is also shown for comparison. It can be seen in Figure 4.5(a) that the relative uncertainty in the neutron dose rates considerably improved when the computation time increased from 800 minutes to 6.4 days, using the analog MCNP simulation. More importantly, the SCALE simulation for a computer time of 800 minutes proved to be the most efficient approach among these three cases. Here, approximately 99.7% of the voxels had a relative uncertainty that was less than 10%. For photon dose rates, the SCALE provided considerably good statistical uncertainties, considering the fact that the contribution of photon dose rates to the total dose rates was not very significant in almost all of the six directions (see Tables 4.1 and 4.2).

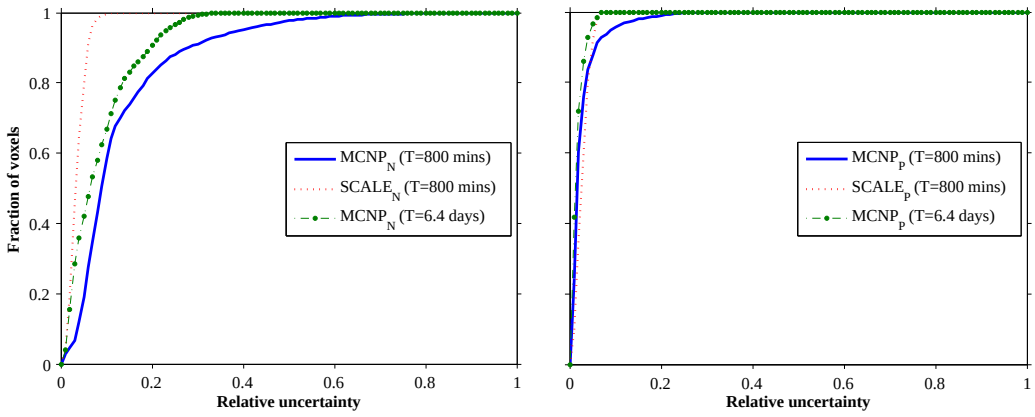

(a) (b)

Figure 4.5 Histograms showing relative uncertainty in dose rates contributed from (a) neutrons and (b) photons.

5. CONCLUSION

A new shielding analysis tool of SCALE6—MAVRIC—with the automatic variance reduction technique of SCALE6, was used to model and simulate the current shielding of the neutron generator installed in the Nuclear Engineering Department of Missouri S&T. The automated variance reduction capability of the MAVRIC yielded an average computational speedup of 11.3 for neutron dose rates with respect to an unbiased MCNP simulation. The neutron and photon dose rates (and their respective uncertainties) at various positions near the facility are discussed and compared.

ACKNOWLEDGMENTS

The work presented in this paper is supported by U.S. NRC under the Award Number NRC-HQ-12-G-38-0039.

REFERENCES

[1] I. Lux and L. Koblinger. *Monte Carlo particle transport methods: neutron and photon calculations*, volume 102. CRC press Boca Raton, 1991.

[2] M.H. Kalos, F.R. Nakache, and J. Celnik. Monte Carlo methods in reactor computations. *Computing methods in reactor physics*, pages 359–438, 1968.

[3] M.H. Kalos and P.A. Whitlock. Monte Carlo methods – Volume I: Basics, 1986.

[4] T.E. Booth. Automatic importance estimation in forward Monte Carlo calculations. *Trans. Am. Nucl. Soc.*, 41(CONF-820609), 1982.

[5] T.E. Booth. Weight window/Importance generator for Monte Carlo streaming problems. Technical report, Los Alamos National Lab., NM (USA), 1983.

[6] T.E Booth and J.S. Hendricks. Importance estimation in forward Monte Carlo calculations. *Fusion Science and Technology*, 5(1):90–100, 1984.

[7] S.N. Cramer and J.S. Tang. Variance reduction methods applied to deep-penetration Monte Carlo problems. Technical report, Oak Ridge National Lab., TN (USA), 1986.

[8] J.C. Wagner and A. Haghighat. Automated variance reduction of Monte Carlo shielding calculations using the discrete ordinates adjoint function. *Nuclear Science and Engineering*, 128(2):186–208, 1998.

[9] A. Haghighat and J.C. Wagner. Monte Carlo variance reduction with deterministic importance functions. *Progress in Nuclear Energy*, 42(1):25–53, 2003.

[10] J.C. Wagner, D.E. Peplow, S.W Mosher, and T.M. Evans. Review of hybrid (deterministic/Monte Carlo) radiation transport methods, codes, and applications at Oak Ridge National Laboratory. *Progress in Nuclear Science and Technology*, pages 808–814, 2010.

[11] D.E. Peplow. Monte Carlo shielding analysis capabilities with MAVRIC. *Nuclear Technology*, 174(2):289–313, 2011.

[12] H.P. Smith and J.C. Wagner. A case study in manual and automated Monte Carlo variance reduction with a deep penetration reactor shielding problem. *Nuclear Science and Engineering*, 149(1):23–37, 2005.

[13] R.D. Sheu, S.H. Jiang, and C.H. Kao. Adjoint acceleration of Monte Carlo simulations using TORT/MCNP coupling approach: a case study on the shielding improvement for the cyclotron room of the Buddhist Tzu Chi general hospital. *Radiation Protection Dosimetry*, 113(2):140–151, 2005.

[14] A.Y. Chen, Y-WH Liu, and R.J. Sheu. Radiation shielding evaluation of the BNCT treatment room at THOR: A TORT-coupled MCNP Monte Carlo simulation study. *Applied Radiation and Isotopes*, 66(1):28–38, 2008.

[15] D.P. Hartmangruber and B. Petrovic. Using SCALE6/MAVRIC to determine the dose rate distribution in the IRIS power plant control room and preliminary estimate throughout the reactor building. *Nuclear Technology*, 175(1):187–197, 2011.

[16] D.L. Williams, J.H. Vainionpaa, G. Jones, M.A. Piestrup, C. K. Gary, J.L. Harris, M.J. Fuller, J.T. Cremer, B.A. Ludewigt, J.W. Kwan, J. Reijonen, K.N. Leung, and R.A. Gough. High intensity, pulsed, DD neutron generator. In *Applications of Accelerators in Research and Industry, Twentieth International Conference, Fort Worth, Texas*, pages 10–15, 2008.

[17] S.S. Nargolwalla and E.P. Przybylowicz. *Activation analysis with neutron generators*. Wiley and Sons, NewYork, 1973.

[18] IAEA Radiation Technology Reports No. 1. Neutron generators for analytical purposes. Technical report, 2012.

[19] J.T. Cremer, D.L. Williams, C.K. Gary, M.A. Piestrup, D.R. Faber, M.J. Fuller, J.H. Vainionpaa, M. Apodaca, R.H. Pantell, and J. Feinstein. Large area imaging of hydrogenous materials using fast neutrons from a DD fusion generator. *Nuclear Instruments and Methods in Physics Research A*, 675:51–55, 2012.

[20] M.K. Fuller, M.A. Piestrup, C. K. Gary, J. L. Harris, G. Jones, J. H. Vainionpaa, D. L. Williams, J. T. Cremer, A. Bell, G. McRae, et al. Long-lifetime high-yield neutron generators using the DD reaction. 2009.

[21] M.K. Sharma, A.B. Alajo, and X. Liu. MCNP modeling of a neutron generator and its shielding at Missouri University of Science and Technology. *Nuclear Instruments and Methods in Physics Research Section A*, 767:126–134, 2014.

[22] MCNP-A general Monte Carlo N-Particle transport code, version 5. Los Alamos National Laboratories, Los Alamos, New Mexico, 2011.

[23] NCRP Report No. 144. Radiation protection for particle accelerator facilities. Technical report, National Council on Radiation Protection and Measurements, Bethesda, MD, 2005.

[24] D.L. Chichester and B.W. Blackburn. Radiation fields from neutron generators shielded with different materials. *Nuclear Instruments and Methods in Physics Research Section B*, 261(1):845–849, 2007.

[25] Y. Elmahroug, B. Tellili, and C. Souga. Calculation of fast neutron removal cross-sections for different shielding materials. *International Journal of Physics and Research*, 3(2):7–16, 2013.

[26] J.E. Turner. *Atoms, radiation, and radiation protection*. John Wiley & Sons, 2008.

[27] R.J. McConn Jr., C.J. Gesh, R.T. Pagh, R.A. Rucker, and R.G. Williams III. Compendium of material composition data for radiation transport modeling. *PNNL-15870 Rev*, 1(4), 2011. URL `http://www.pnnl.gov/main/publications/external/technical_reports/PNNL-15870Rev1.pdf`.

[28] SCALE: A comprehensive modeling and simulation suite for nuclear safety analysis and design. *ORNL/TM-2005/39, Version 6.1*, June 2011.

[29] D.J. Whalen, D.A. Cardon, J.L. Uhle, and J.S. Hendricks. MCNP: Neutron benchmark problems. Technical report, Los Alamos National Lab., NM (United States). Funding organization: USDOE, Washington, DC (United States), 1991. URL `http://www.iaea.org/inis/collection/NCLCollectionStore/_Public/23/033/23033166.pdf`.

[30] E.E. Lewis and W.F. Miller. Computational methods of neutron transport. 1984.

[31] X-5 Monte Carlo Team. MCNP-A general Monte Carlo N-Particle transport code, version 5. 2003.

IV. INTEGRATED DOSES CALCULATION IN EVACUATION SCENARIOS OF THE NEUTRON GENERATOR FACILITY AT MISSOURI S&T

Manish K. Sharma, Ayodeji B. Alajo

Missouri University of Science & Technology,

Nuclear Engineering, Rolla, MO, USA

ABSTRACT[¶]

Any source of ionizing radiations could lead to considerable dose acquisition to individuals in a nuclear facility. Evacuation may be required when elevated levels of radiation is detected within a facility. In this situation, individuals are more likely to take the closest exit. This may not be the most expedient decision as it may lead to higher dose acquisition. The strategy followed in preventing large dose acquisitions should be predicated on the path that offers least dose acquisition. In this work, the neutron generator facility at Missouri University of Science and Technology was analyzed. The Monte Carlo N-Particle (MCNP) radiation transport code was used to model the entire floor of the generator's building. The simulated dose rates in the hallways were used to estimate the integrated doses for different paths leading to exits. It was shown that shortest path did not always lead to minimum dose acquisition and the approach was successful in predicting the expedient path as opposed to the approach of taking the nearest exit.

Keywords: Integrated doses, Dosimetry, Radiation exposure, Neutron generator, Emergency planning

---

[¶]Published in Nuclear Instruments and Methods in Physics Research Section A (2016).

1. INTRODUCTION

Any extraneous radioactive source exposed intentionally or accidentally may represent high dose rates in a nuclear facility. Likewise, any accidental operation of equipment producing ionizing radiations (e.g., a neutron generator) may lead to large dose acquisition to personnel in the facility. In an event that requires evacuation, individuals are more likely to take the nearest exit. In a facility with more than one exit pathway, it is possible that the nearest exit may not offer the pathway to the least radiation exposure. The approach and prediction should be decided based on the route that leads to minimum dose acquisition.

There are existing publications and tools for predicting dose acquisitions. A set of computational tools to estimate the integrated doses associated with maintenance activities at National Ignition Facility (NIF) is discussed in [1]. The Automated ALARA-MCNP Interface (AAMI) and NIF Exposure Estimation Tool (NEET) are used for work planning and estimating the integrated doses. The AAMI code creates dose rate maps through a series of calculations. NEET is a web application that can perform radiation exposure calculations to compute the dose rate maps—which is valuable for planning purposes. Additional information about maintenance activities at NIF, and NEET is available in [2]. The intervention doses for the CNGS (CERN Neutrinos to Gran Sasso) facility are estimated in [3]. These calculations are integral in cases where a human, instead of a robot, intervention is obligatory. Fabry et al. [4, 5] discusses the issue of minimizing integrated dose acquired during maintenance operations. They present a software program to plan and optimize the maintenance interventions in a facility with ionizing radiation. The software automatically computes the expected dose acquisition by the maintenance workers.

Estimation of integrated doses in the areas of intervention is vital to establish the radioprotection measures for the personnel in accordance with the As Low as Reasonably Achievable (ALARA) radiation safety principle. Any proactive planning, optimization, and estimation of integrated doses is key in prevention of large dose acquisitions, especially in

evacuation scenarios of facility with well-understood characteristics [6]. In this work, the integrated doses in a neutron generator facility at Missouri University of Science and Technology (Missouri S&T) were computed. A previously developed model of the generator and its shielding was extended to cover the entire floor of the building using the Monte Carlo N-Particle (MCNP) radiation transport code [7]. The simulated dose rates were used to estimate the integrated doses for different cases using MATLAB. Unlike the tools and methods described in [1, 3], which are developed to calculate in-situ doses over a period of residence, the approach herein is focused on evacuation scenarios and is similar to [4, 5]. While the work presented in [4, 5] is centered on trajectory optimization during maintenance interventions, the proposed work is motivated by the need of expedient decisions in responding to emergency and evacuation scenarios. The results of this work are crucial to prevent and mitigate large dose acquisitions in accidental-operation scenarios at Missouri S&T generator facility.

2. FACILITY LAYOUT AND MCNP MODELING

The layout of second floor of Fulton Hall building is shown in Figure 2.1. The numbers represent the different rooms and laboratories of Nuclear Engineering department at Missouri S&T. A DD-109 accelerator-type neutron generator is located in room 217A (shown in red star). The generator utilizes deuterium-deuterium fusion reactions (^{2}H + ^{2}H $\rightarrow$ ^{3}He + n) to produce neutrons of approximate energy 2.5 MeV. The working of neutron generator and its applications can be found in [8, 9]. The generator is surrounded with different materials to reduce the dose rates in the vicinity of the room. The details and the developed models of neutron generator and its shielding are extensively discussed in [7, 10]. The MCNP model of neutron generator, its shielding and room was extended to cover the entire floor. For simplification, the peripheral rooms of the floor (e.g., rooms 222A, 223-227, etc. in Figure 2.1) were not included in the final model. This was a fair assumption since the goal was to determine the dose rates in the hallways (shaded with gray color in Figure 2.1). Any contribution in dose rates from structures that do not fall within the direct line-of-sight of the generator (to the hallways) was ignored. However, walls physically present along the boundary of exclusion were modeled to account for albedo effects. The dimensional and compositional details of walls, floor, and the roof [7, 10–12] were then used to create a geometric model. A two-dimensional (xy) and a three-dimensional view of the model, obtained using MCNPX visual plotter [13], are shown in Figures 2.2 and 2.3, respectively.

2.1 MCNP SIMULATION OF FULTON HALL'S SECOND FLOOR MODEL

A point source of neutron generation was assumed to be emitting 2.5 MeV neutrons isotropically with an intensity 2×10^9 neutrons/s and an MCNP transport simulation was performed for 8×10^9 particle histories. Several FMESH tallies with different bin sizes were created in the hallways to see the impact of bin size on relative uncertainties in dose rates. Bins of sizes 5 cm $\times$ 5 cm, 10 cm $\times$ 10 cm, 12.5 cm $\times$ 12.5 cm, 25 cm $\times$ 25 cm, and

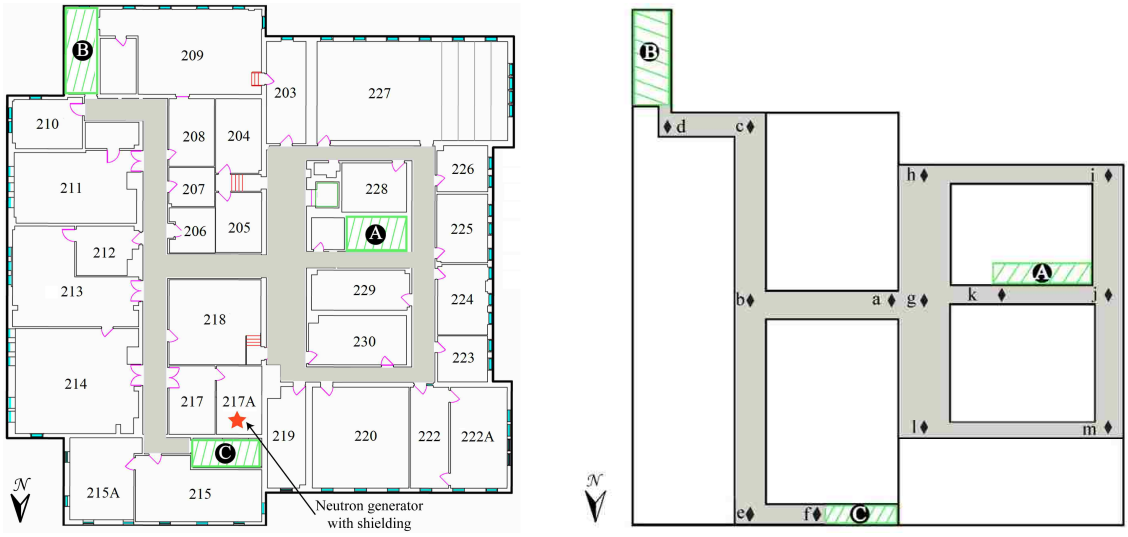

Figure 2.1 Fulton Hall's second floor where the neutron generator is located. (a) Shown in red star is the generator (with its shielding). The three exits of the floor—A, B, and C—are shown and hallways leading to these exits are shaded. (b) Hallways with major nodes indicated.

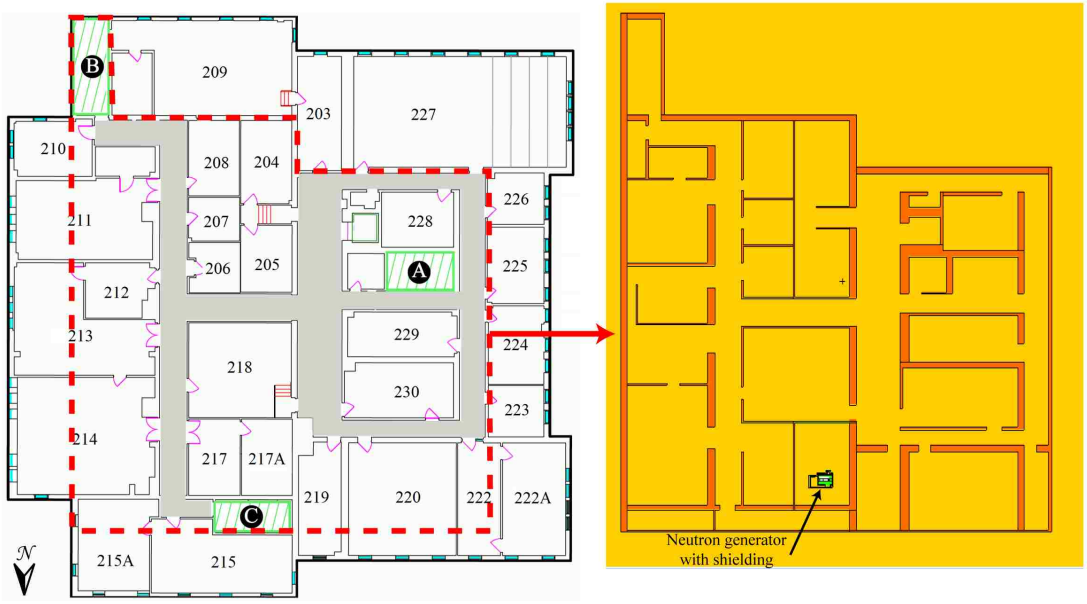

Figure 2.2 MCNP model of Fulton Hall's second floor. Hallways leading to different exits are shaded in gray.

50 cm $\times$ 50 cm were created in the $x \times y$ directions. The size of each tally was kept 10 cm in the z direction. Further, the tallies were created along the central plane passing through the neutron source—where the dose rates were expected to be the highest. The simulations utilized the appropriate fluence-to-dose conversion factors for neutrons and photons based on ICRP publication 116 [14]. The computation time of each simulation was approximately 8 days on a computer system with an Intel Core-i7 3.70 GHz processor and a 32 GB RAM with eight threads. The total dose rate (i.e., the sum of neutron and photon dose rates) at various nodes in the hallways is represented and discussed in section 4.

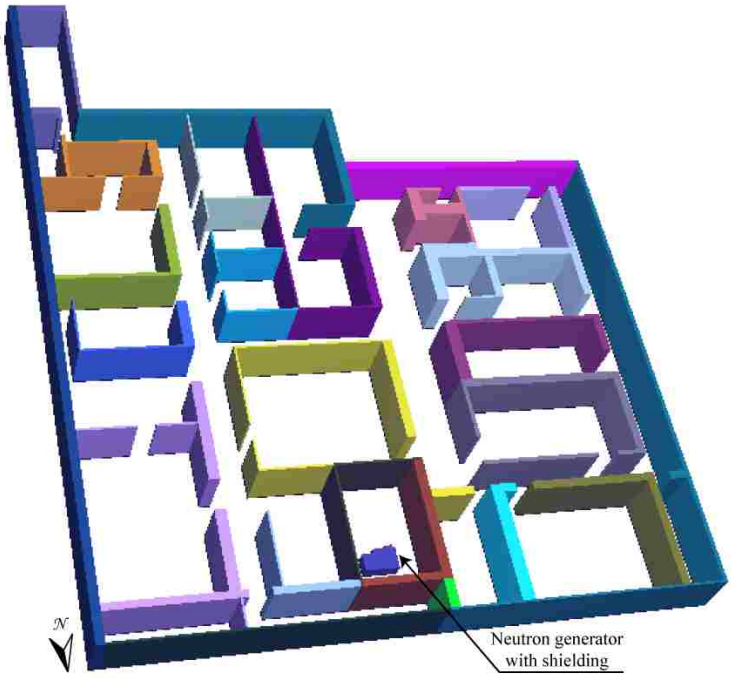

Figure 2.3 Three-dimensional view of the MCNP model obtained using MCNPX visual plotter [13]. Roof and floor are not shown for spatial clarity.

3. APPROACH FOR INTEGRATED DOSE CALCULATION

The integrated dose calculation is performed using the simulated dose rates. The integrated dose acquired in any path is a summation of contributions from the different nodes traversed. The approach is similar to the mathematical model presented by Fabry et al. [4, 5]. The integrated dose between any two nodes, x_1 and x_n, is given by

$$D_{1n} = \dot{D}_{12} * \frac{\Delta x}{|v|} + \dot{D}_{23} * \frac{\Delta x}{|v|} + \ldots + \dot{D}_{(n-1)n} * \frac{\Delta x}{|v|} \tag{4}$$

where $x_1, x_2, \ldots, x_n$ are different but equidistant nodes encountered in any particular path, Δx is the distance between any two consecutive nodes, and v is the velocity of the person (see Figure 3.1). $D_{(i-1)i}$ for $i = 2, 3, \ldots, n$, represents the average of dose rates at the consecutive nodes $(i-1)$ and i.

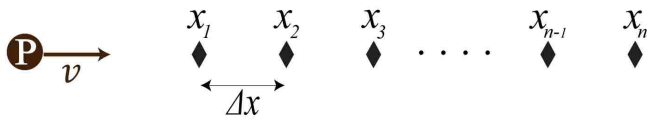

Figure 3.1 Different nodes traversed in a particular path. A person at position P was assumed moving with velocity v.

Equation (4) implicitly assumes that the person is constantly moving at a fixed speed along the nodal line (in this work, $v = 2$ ms^{-1} was assumed). Equation (4) calculates the integrated dose for each possible path and person (or clusters of persons) in different regions of the floor. These values are finally compared to distinguish the route with least dose acquisition. This approach is implemented using MATLAB (see Figure 3.2). The neutron and photon uncertainties in dose rates at each node are also known and error propagation [15] is used to determine the propagated uncertainty in the integrated doses. It is important to note that the integrated dose is inversely proportional to the speed of travel. As long as an

individual maintains a particular speed in the facility, the safest path will remain the same for the individual. A speed factor, $f_{(v,j)}$, for an individual is defined as the scale-up factor for the speed in order to match the minimum dose possible if the nearest exit is taken.

$$f_{v,j} = \frac{D_{nearestexit,j}}{D_{min,j}} \tag{5}$$

where $D_{(nearestexit,j)}$ is the dose acquired if the nearest exit is taken from starting location P_j and $D_{(min,j)}$ is the minimum dose acquired through any exit from P_j.

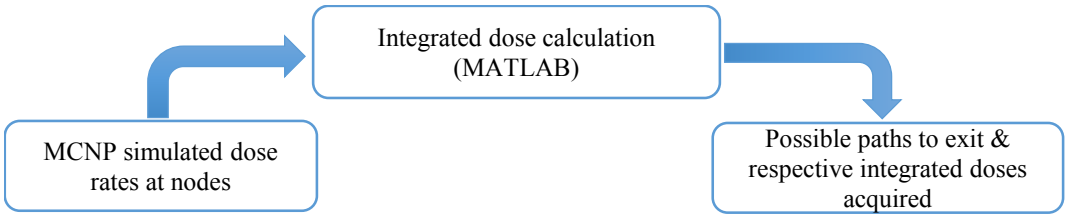

Figure 3.2 Integrated dose calculation using the simulated dose rates at various nodes in the hallways.

4. RESULTS AND DISCUSSION

Figure 4.1 shows histograms of relative uncertainties in neutron and photon dose rates for different tally-bin sizes. As expected, a larger bin size offered better statistical uncertainties—since more particles were registered in that bin. For the 50 cm bin size, approximately 99% of the voxels had neutron dose rate uncertainties less than 20% (see Figure 4.1(a)). It was previously concluded that the neutrons' contribution in total dose rates was significantly higher than the photons' contribution [7, 10]. Hence the dose rates for 50 cm tally size were chosen for integrated dose calculation—the total dose rate at different nodes are shown in Figure 4.2. Note that the coordinate system was centered at the point where neutrons were created in the generator and the nodes closer to the source had relatively higher dose rates. The approach, implemented in MATLAB, used these values to list the different possible paths and corresponding integrated doses to exit. Three different cases, of persons at three different locations (P_I, P_{II}, and P_{III}), were analyzed (see Figure 4.3) and the results are given in Table 4.1.

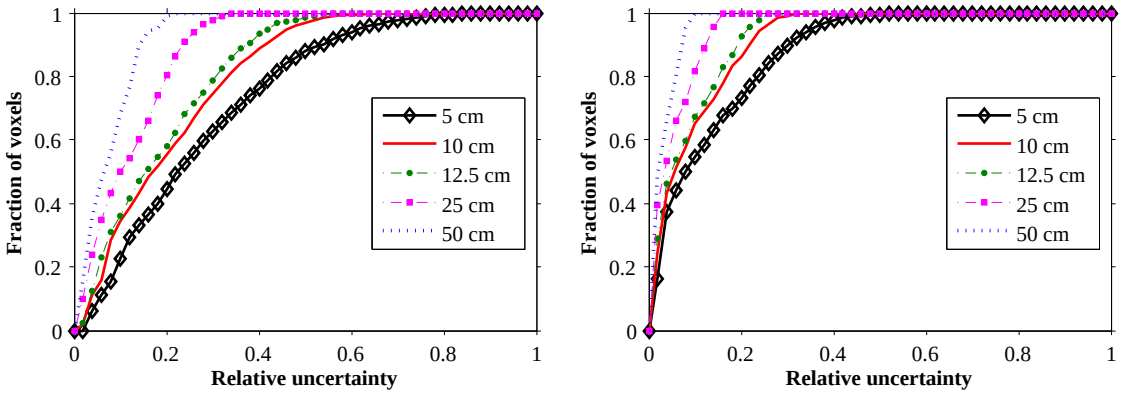

Figure 4.1 Histograms of relative uncertainties in (a) neutron and (b) photon dose rates.

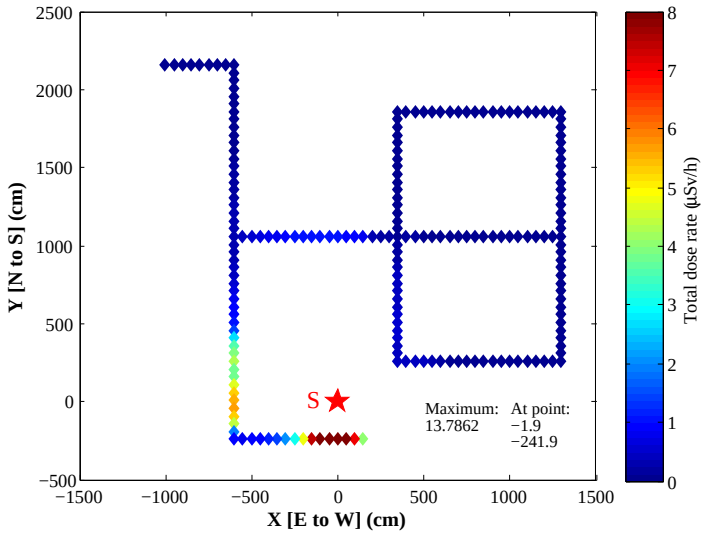

Figure 4.2 Total dose rate at various nodes. Each node is 50 cm apart from its consecutive node. Neutron source at origin is shown by red star.

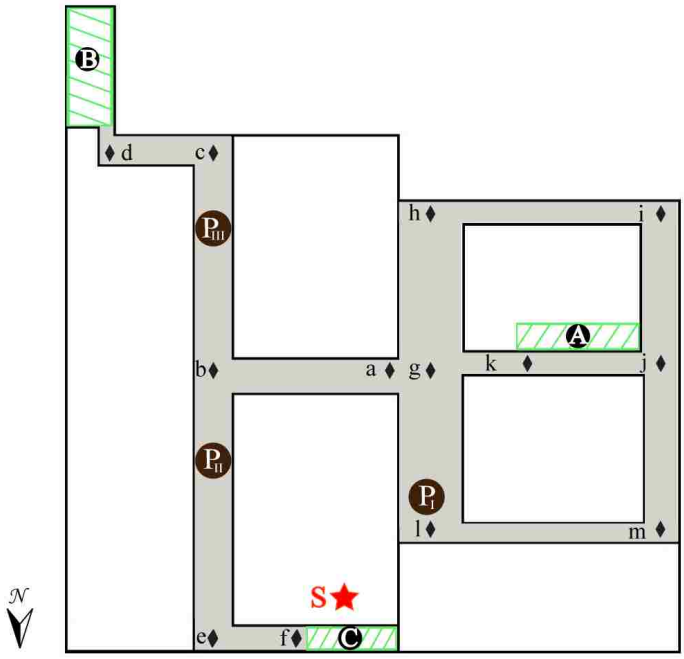

Figure 4.3 Three different cases of persons at three different locations: P_I, P_{II}, and P_{III}. The position P_I overlaps the node l. However, it is shown separately for spatial clarity. Major nodes are indicated in diamonds.

The shortest path to the exit did not always lead to least dose acquisition (see Table 4.1). For example, in case I (of a person at position P_I), the approach to take exit A through path A_3 (primarily because path A_3 was the shortest) led to higher dose acquisition. However, the integrated dose significantly dropped when the decision was based on integrated doses—i.e., path A_1. The dose acquisition reduced to approximately 43% of one obtained with the path A_3 (202/471 = 0.43). The distance traversed, however, was approximately 1.7 times which was immaterial—since the objective was to minimize the dose acquisition in accordance with the ALARA principle. If the shortest route is taken, a speed factor of 2.3 is needed to match the acquired dose to the minimum value. A speed of 4.6 ms^{-1} is practically achievable if the shortest route is taken by an evacuee in order to limit dose acquisition to the minimum achievable at a speed of 2 ms^{-1}. The integrated doses to exit B were relatively higher compared to exit A, primarily because the person spent more time in the regions with higher dose rates. The integrated doses to exit C were the highest among the three exits. This was due to its proximity to the neutron generator and the person effectively moved into a radiation-prone area. Therefore, the safest route in case I was to take exit A through the path A_1 in the west direction.

In case II, B_1 led to least dose acquisition although this path was approximately 1.4 times longer than the shortest path, C_1 (20.6/14.9 = 1.4). However, the dose acquired in path B_1 was approximately 14 times lower (9590/662 = 14.5) since the person continuously moved out of the radiation zone. Therefore, in this case, path B_1 to exit B was deemed safest. The speed factor in this case was 14.5 and a speed of 29 ms^{-1}, which is impractical to achieve without the aid of a transportation device. Similarly, path B_1 through nodes *c* and *d* led to least dose acquisition for case III. It is worth noting that exit B was coincidentally at the shortest distance from the person; hence the speed factor was unity. The average time taken by MATLAB for these three cases was in between 0.02-0.04 seconds on a computer system with 2.20 GHz Intel Core2 Duo processor and 2.0 GB installed RAM.

Table 4.1 Integrated dose and distance for each path. The speed factor for each case is also given.

Case	Exit	Path to exit		Distance to exit (m)	Integrated dose (pSv)	$f_{v,j}$
		Path name	Major nodes traversed			
I (Person at P_I)	A	A_1	l-m-j-k	22	202 ± 1	2.3
		A_2	l-m-i-h-g-k-A	48	311 ± 1	
		A_3	l-g-k-A	13	471 ± 1	
	B	B_1	l-m-j-b-c-d-B	51.5	1449 ± 3	
		B_2	l-m-i-h-g-b-c-d-B	67.5	1469 ± 3	
		B_3	l-g-b-c-d-B	32.5	1629 ± 3	
	C	C_1	l-m-j-b-e-f-C	51.5	11276 ± 9	
		C_2	l-m-i-h-g-b-e-f-C	67.5	11297 ± 9	
		B_3	l-g-b-e-f-C	38	11457 ± 9	
II (Person at P_{II})	A	A_1	b-a-g-k-A	20.1	1494 ± 3	14.5
		A_2	b-a-g-l-m-j-k-A	45.1	2079 ± 4	
		A_3	b-a-g-h-i-j-k-A	45.1	1550 ± 3	
	B	B_1	b-c-d-B	20.6	662 ± 2	
	C	C_1	e-f-C	14.9	9590 ± 8	
III (Person at P_{III})	A	A_1	b-a-g-k-A	20.9	1217 ± 3	1.0
		A_2	b-a-g-l-m-j-k-A	45.9	1802 ± 3	
		A_3	b-a-g-h-i-j-k-A	45.9	1272 ± 3	
	B	B_1	c-d-B	8.6	30 ± 1	
	C	C_1	b-e-f-C	26.9	10213 ± 9	

In all of the three cases, it was observed that the shortest route did not always lead to least dose acquisition. The decision to exit or evacuate the facility was solely based on the path that was deemed safest by the scheme. It is possible that the same exit is suggested to several persons in the facility. In these circumstances, a better decision should be made to re-route some of these persons to avoid any unnecessary traffic (hence, dose acquisition) at

any exit. It is also worth noting that the safest route for each case did not change even when dose rates from other tallies (of different bin sizes) were used in integrated dose calculation. The integrated doses for other tallies were within 9.6% of the ones given in Table 4.1.

5. CONCLUSION

In this paper, an MCNP model of a neutron generator and its shielding was extended to cover the entire floor of the building at Missouri University of Science and Technology. The simulated dose rates in the hallways were used to estimate the integrated dose for different paths and cases. The approach successfully distinguished the safest path—with least dose acquisition—for different cases of persons at different locations of floor.

Some of the considerations that have not been the focus of this work are the following:

- ⋆ communicating the safest route with the evacuees
- ⋆ overloading a particular exit
- ⋆ variation in exit speed of individuals and between individuals
- ⋆ situation leading to stalling of evacuee's egression

These considerations are important for actualization of strategy discussed in this paper.

ACKNOWLEDGEMENTS

The work presented in this paper is supported by U.S. NRC under the Award Number NRC-HQ-11-G-38-0008.

REFERENCES

[1] J. Verbeke. Planning tools for estimating radiation exposure at the National Ignition Facility. *Fusion Science and Technology*, 60(2):595–599, 2011.

[2] H. Khater, S. Brereton, L. Dauffy, J. Hall, L. Hansen, S. Kim, T. Kohut, B. Pohl, S. Sitaraman, J. Verbeke, and M. Young. Analysis of decay dose rates and dose management in the National Ignition Facility. *Health Physics*, 104(6):580–588, 2013.

[3] M.L. Sentís, A. Ferrari, and S. Roesler. Calculation of intervention doses for the CNGS facility. *Nuclear Instruments and Methods in Physics Research Section A*, 562 (2):985–988, 2006.

[4] T. Fabry, L. Vanherpe, M. Baudin, C. Theis, C. Braesch, and B. Feral. Interactive intervention planning in particle accelerator environments with ionizing radiation. *Nuclear Instruments and Methods in Physics Research Section A*, 708:32–38, 2013.

[5] T. Fabry, J. Blaha, L. Vanherpe, C. Braesch, L. Tabourot, and B. Feral. The practical use of an interactive visualization and planning tool for intervention planning in particle accelerator environments with ionizing radiation. *Nuclear Instruments and Methods in Physics Research Section A*, 743:14–21, 2014.

[6] M. Crick. Nuclear and radiation safety: guidance for emergency response. *IAEA Bulletin*, 38(1):23–27, 1996.

[7] M.K. Sharma, A.B. Alajo, and X. Liu. MCNP modeling of a neutron generator and its shielding at Missouri University of Science and Technology. *Nuclear Instruments and Methods in Physics Research Section A*, 767:126–134, 2014.

[8] S.S. Nargolwalla and E.P. Przybylowicz. Activation analysis with neutron generators. 1973.

[9] Neutron generators for analytical purposes. *IAEA Radiation Technology Reports No. 1*, 2012.

[10] M.K. Sharma, A.B. Alajo, and X. Liu. Adjoint acceleration of Monte Carlo simulations using SCALE: A radiation shielding evaluation of the neutron generator room at Missouri S&T. *Nuclear Instruments and Methods in Physics Research Section A*, 792:47–55, 2015.

[11] R.J. McConn Jr., C.J. Gesh, R.T. Pagh, R.A. Rucker, and R.G. Williams III. Compendium of material composition data for radiation transport modeling. *PNNL-15870 Rev*, 1(4), 2011.

[12] D.J. Whalen, D.A. Cardon, J.L. Uhle, and J.S. Hendricks. *MCNP: Neutron benchmark problems*. Los Alamos National Laboratory, 1991.

[13] MCNP–A General Monte Carlo N-Particle Transport Code, Version 5. *Los Alamos National Laboratory, Oak Ridge, TN*, 2011.

[14] Conversion coefficients for radiological protection quantities for external radiation exposures. *ICRP Report No. 116*, 40(2-5), 2010.

[15] G.F. Knoll. *Radiation detection and measurement*. John Wiley & Sons, 2010.

SECTION

2. CONCLUSION

The dissertation presents concepts and schemes that could be integrated to prevent and mitigate large dose acquisitions in radiation-prone facilities. Primarily, the work was divided into three segments: (i) localize the gamma-ray radioactive source, (ii) predict the impact over a region of interest, and (iii) distinguish the safest path to exit the facility. Following are the important conclusions of this work.

- ⋆ The localization algorithm, developed using statistic-based grid-refinement methodology, was verified with the MCNP radiation transport simulation. The accuracy in this case was 5 μm. In the experimental validation of the algorithm with five detector positions, a weak ^{137}Cs source (of activity 5.1 μCi) was predicted with an accuracy of 53 cm for a measurement time of 3 min. The accuracy improved and stabilized to approximately 25 cm for higher measurement times. Since the algorithm localized the weak source in 3 min, it is believed that it can localize higher activity sources (commonly encountered in nuclear facilities) in real-time—assuming the same physical placement of source and detectors.

- ⋆ The accelerator-type neutron generator was modeled using MCNP and SCALE codes. The dose rates obtained from these two independent simulations, and from the analytical calculation, were in agreement. The speedup of accelerated Monte Carlo simulation (using MAVRIC sequence in SCALE package) is cardinal in near real-time impact prediction (dose-mapping) in the facility.

- ⋆ The generator model was further extended to cover the entire floor of Fulton Hall's building. The goal was to estimate the dose rates in the hallways and test the dose reduction approach. The approach calculated the integrated doses for different paths

and distinguished the safest path to exit the building. The approach, therefore, was successful in predicting the expedient path as opposed to the approach of taking the nearest exit.

REFERENCES

[1] MCNP-A general Monte Carlo N-Particle transport code, version 5. Los Alamos National Laboratories, Los Alamos, New Mexico, 2011.

[2] I. Takumi, M. Nagai, S. Kato, M. Hata, and H. Yasukawa. Estimation of EM source location from 223 Hz EM field power data at multiple spots. In *Geoscience and Remote Sensing Symposium, 2001 (IGARSS'01). IEEE 2001 International*, volume 7, pages 3191-3193, IEEE, 2001.

[3] SCALE: A comprehensive modeling and simulation suite for nuclear safety analysis and design. *ORNL/TM-2005/39, Version 6.1,* June 2011.

VITA

Manish Sharma was born and brought up in India. He obtained his Bachelor of Technology degree in Electrical Engineering in the year 2009. He was in top 2.1% of the students to receive fellowship from Ministry of Human Resource and Development, India, and pursue his masters in Nuclear Engineering from Indian Institute of Technology Kanpur. As a Ph.D. student, Manish joined Missouri University of Science and Technology (Missouri S&T) in the year 2011. He earned his Ph.D. degree in July 2016 and was one of the eleven students who were awarded Dissertation Completion Fellowship at Missouri S&T. Manish has also played an integral role in several campus and departmental activities and has led MATLAB and Monte Carlo sessions. He was one of the five graduate students who were selected from Missouri S&T to attend various leadership meetings led by University of Missouri System (Rolla, St. Louis, Columbia, and Kansas City). He was honored as the "Best Department Representative" by the Missouri S&T Council of Graduate Students, and he was actively involved in Nuclear Engineering Summer Camps, Introduction to Engineering Jackling Camps, Science Olympiad, and First Tech Championship.